Drosophila Tropomodulin is required for multiple actin-dependent processes in myofiber assembly and maintenance

Carolina Zapater i Morales[1,2], Peter J. Carman[3,4], David B. Soffar[2], Stefanie E. Windner[2], Roberto Dominguez[3,4], and Mary K. Baylies[1,2,5].

1. Biochemistry, Cell & Developmental Biology, and Molecular Biology (BCMB) program, Weill Cornell Graduate School of Medical Sciences, New York, NY 10065
2. Developmental Biology Program, Sloan Kettering Institute, Memorial Sloan Kettering Cancer Center, New York, NY 10065
3. Biochemistry and Molecular Biophysics Graduate Group, Perelman School of Medicine, University of Pennsylvania, Philadelphia, PA 19104
4. Department of Physiology, Perelman School of Medicine, University of Pennsylvania, Philadelphia, PA 19104
5. Lead contact (Correspondence: bayliesm@mskcc.org)

Keywords: Skeletal muscle, Tropomodulin (Tmod), *Drosophila*, sarcomere length, myofibril orientation, tension-mediating proteins, misshapen nuclei.

SUMMARY STATEMENT

Drosophila Tropomodulin knockdown in larval myofibers results in myopathy-related phenotypes. Our findings support that Tmod acts in actin-related processes at different subcellular locales, all critical for muscle integrity and function.

ABSTRACT

Proper muscle contraction requires the assembly and maintenance of sarcomeres and myofibrils. While the protein components of myofibrils are generally known, less is known about the mechanisms by which they individually function and together synergize for myofibril assembly and maintenance. For example, it is unclear how the disruption of actin filament (F-actin) regulatory proteins leads to the muscle weakness observed in myopathies. Here, we show that knockdown of *Drosophila* Tropomodulin (Tmod) results in several myopathy-related phenotypes, including reduction of muscle cell (myofiber) size, increased sarcomere length, disorganization and misorientation of myofibrils, ectopic F-actin accumulation, loss of tension-mediating proteins at the myotendinous junction, and misshaped and internalized nuclei. Our findings support and extend the tension-driven self-organization myofibrillogenesis model. We show that, like its mammalian counterpart, *Drosophila* Tmod caps F-actin pointed-ends, and this activity is critical for cellular processes in different locations within the myofiber that directly and indirectly contribute to the maintenance of muscle function. Our findings provide significant insights to the role of Tmod in muscle development, maintenance, and disease.

INTRODUCTION

Skeletal muscle cells (myofibers) are essential for survival. Myofibers are comprised of myofibrils, each consisting of arrays of repeating units known as sarcomeres, the muscle's fundamental contractile machinery. These contain three main structural elements: thin filaments, thick filaments, and Z-discs [reviewed in Sweeney and Hammers (2018)]. Z-discs are the thin filament attachment site and are composed of many proteins (e.g.: α-actinin and Zasp). Thin filaments are comprised primarily of actin filaments (F-actin) and actin binding proteins, including proteins important for anchorage to the Z-disc (e.g.: CapZ), for contraction (e.g.: troponin and tropomyosin), and for F-actin length regulation (e.g.: nebulin and Tmod) [reviewed in Szikora et al. (2022), Ghosh and Fowler (2021), Fowler and Dominguez (2017)]. Thick filaments are composed primarily of myosin and myosin-associated proteins. Thin filaments sliding past thick filaments brings Z-discs closer together (contraction), generating force in a calcium-regulated manner. While much is known about protein composition and function of sarcomeres and myofibrils, the mechanisms controlling their formation and maintenance remain elusive.

Although myofibrillogenesis is not well understood, the most widely accepted model suggests tension is essential. According to this model, once the myofiber has attached to tendon cells, short F-actin stochastically attach to each other and to the myofiber ends via tension-activated proteins such as β-Integrin and Talin. Through a positive feedback loop, initial tension attracts more tension-activated proteins, leading to further tension and myofibril assembly and maturation along the myofiber's longitudinal axis (Lemke and Schnorrer, 2017, Lemke et al., 2019, Pines et al., 2012, Weitkunat et al., 2014, Sparrow and Schock, 2009). Subsequently, additional growth and organization along myofibrils also require tension (LeGoff and Lecuit, 2015). Several other processes regulate myofibrillogenesis and myofibril maintenance. Firstly, mitochondria influence myofibrillogenesis and vice versa via the mechanical interplay between mitochondrial dynamics and myofibril morphogenesis (Avellaneda et al., 2021). Secondly, myofibrils undergo protein turnover without compromising their organization during contraction and myofibrillogenesis (Sanger and Sanger, 2008, Ono, 2010, Littlefield and Fowler, 2008). Finally, actin regulatory proteins that control monomeric (G-actin) to F-actin ratios in the cell are critical for myofibril assembly and turnover (Littlefield and Fowler, 2008, Deng et al., 2021). While contributing factors to myofibril formation and maintenance have been identified, their interplay and molecular mechanisms are incompletely understood.

Mutations in sarcomere genes are linked to skeletal muscle diseases such as nemaline myopathy (NM), which presents with muscle weakness (de Winter and Ottenheijm, 2017, Sewry et al., 2019). NM is associated specifically with mutations in thin filament genes, including ACTA1, NEB, LMOD3, CFL2, TPM2, TPM3, TNNT1, TNNT3 and MYPN [reviewed in Laitila and Wallgren-Pettersson (2021), Christophers et al. (2022)]. In addition to the growing list of mutations identified in human patients, Tmod mutant zebrafish show a NM-like phenotype (Berger et al., 2014). Studies in model systems have demonstrated that Tmod regulates F-actin length by capping pointed-ends to inhibit monomer addition/dissociation (Molnar et al., 2014, Berger et al., 2022, Littlefield et al., 2001). Tmod is related in sequence and structure to Leiomodin (Lmod), an F-actin nucleator [(Chereau et al., 2008) and reviewed in Fowler and Dominguez (2017), Yamashiro et al. (2012)], whose deficiency has been linked to NM (Yuen et al., 2014, Cenik et al., 2015). Some Tmods also have low nucleation activity (Fischer et al., 2006, Yamashiro et al., 2010, Yamashiro et al., 2014). While humans have four *TMOD* and three *LMOD* genes that cap and nucleate F-actin, respectively, *Drosophila* has no Lmod, but expresses 18 Tmod splice variants. It is unknown, however, which Tmod isoforms are most abundant in *Drosophila* muscle and whether individual isoforms cap or nucleate F-actin. It is also unknown whether and how the disruption of Tmod isoforms in *Drosophila* would result in the NM-like defects observed in other models.

Previous muscle research focused on the role of Tmod and Lmod in regulating sarcomeric F-actin. However, similar to other cell types, cytoplasmic F-actin plays several essential roles in myofibers: maintenance of intracellular structure by tethering myofibrils to the plasma membrane and extracellular matrix (ECM), organization of myofiber organelles and vesicle trafficking, and movement and anchoring of myonuclei at the myofiber periphery [reviewed in Davidson and Cadot (2021), Charvet et al. (2012), Kee et al. (2009)]. The disruption of cytoplasmic F-actin dynamics could contribute to muscle deterioration and weakness and has not been comprehensively studied. Here, we analyze the effects of Tmod knockdown (Tmod-KD) in *Drosophila* larval muscle. We observe progressive muscle deterioration structurally and functionally, with defects in muscle size, sarcomere length, myofibril homeostasis, integrin-based myofibril attachment, and myonuclear shape and activity. Alongside with myofibrillar organization breakdown, Tmod-KD myofibers show ectopic F-actin accumulations. Transcriptomic analyses reveal downregulation of proteasomal degradation and upregulation of oxidative metabolism. Biochemically, *Drosophila* Tmod exclusively acts as an actin capping protein which, in addition to regulating thin filament length, is involved in establishing tension along the myofiber. The phenotypes generated by Tmod loss support and extend the leading hypothesis of

112 myofibrillogenesis and suggest a role for Tmod in myofibril assembly and maintenance. We
113 propose that Tmod's function as an F-actin capping protein is critical in a variety of locations within
114 the myofiber that directly and indirectly maintain muscle function.
115

RESULTS

Drosophila Tmod is required for larval muscle integrity

To identify genes with a critical role in muscle development and disease, we performed a limited screen in *Drosophila melanogaster*. We used a muscle-specific driver (*Dmef2-Gal4*) and available RNAi lines to knock down homologues of human proteins implicated in myofibril/sarcomere structure and function (Schnorrer et al., 2010) (Table S1). We screened for embryonic lethality, muscle defects in late third instar larvae, pupal lethality, and adult flight (Table S2). Expression of *tmod*RNAi resulted in phenotypes that suggested Tmod maintains muscle integrity and function. We confirmed the KD phenotypes using three different RNAi lines and a homozygous *tmod* mutant, and assessed KD levels by qRT-PCR, immunofluorescence, and Western blot (Fig. S1). Based on these results, we selected *tmod* for further study and used one RNAi line, dsRNA-HMS02283 (Perkins et al., 2015), for subsequent KD experiments as it exhibited an intermediate phenotype and degree of mRNA KD.

Drosophila larvae are segmented organisms with three thoracic and eight abdominal body segments (A1-A8), each consisting of ~30 unique body muscles (Bate, 1990). Here, we focused on two ventral longitudinal (VL) muscles, VL3 and VL4 (also named muscles 6 and 7), which are well characterized, easily assessable, flat rectangular cells with nuclei located on one cell surface (Fig. 1A-C) (Windner et al. (2019). Muscle-specific Tmod-KD resulted in a striking phenotype at the end of larval development, with a significant reduction in myofiber size (Fig. 1D,E). While the myofiber length was conserved, the width was reduced by 30-60% (Fig. 1D-F). Furthermore, we observed several distinct morphological features: increased sarcomere length (Fig. 1G), disorganized, misoriented myofibrils (Fig. 1I), ectopic F-actin accumulation (Fig. 1D,E), and misshaped, internalized nuclei (Fig. 1J). Strikingly, intact myofibrils with changes in sarcomere length were restricted to the myofiber's cuticular side. In contrast, the myofiber's visceral surface, which includes the myonuclei, was disorganized (Fig. 1E). These observations supported a crucial function for Tmod in regulating sarcomeric actin and myofibril stability. Furthermore, they suggested additional Tmod role(s) in the regulation of cytoplasmic actin, including nuclear stabilization and other cellular processes.

Tmod-KD myofibers deteriorate in a specific pattern

Drosophila larval development can be divided into four instar stages during which body wall muscles grow dramatically in size (25 to 40-fold): first, second, early third, and late third instars (the last two hours of which is called the "wandering" stage). Over this four-day period, new

150 sarcomeres and myofibrils are added, while nuclear number remains constant (Demontis and
151 Perrimon, 2009, Bai et al., 2007, Balakrishnan et al., 2020). While muscle phenotypes were found
152 in all Tmod-KD late third instars (see also Fig. S1B), not all segments were affected equally.
153 Instead, we found a gradient of muscle phenotypes along the larval anterior-posterior (AP) axis.
154 Myofibers in more anterior segments (A1, A2) had severely disrupted myofibrils and nuclei, while
155 posterior ones (A5, A6) maintained nuclear shape and position and exhibited a milder myofibrillar
156 phenotype.
157
158 We analyzed Tmod-KD phenotypes along the larval AP axis throughout larval development. In
159 first instars, we observed wildtype (WT)-like muscles, which contained the typical conserved
160 arrays of sarcomeres. The first observed defects in the Tmod-KD myofibers were diagonal
161 myofibrils at the myofiber ends of segments A1 and A2 in second instars (Fig. 2A; Fig. S2). In
162 early third instars, these defects also appeared in mid-segments (A4, A5) and became even more
163 pronounced in the anterior segments, which displayed ectopic diagonally intersecting myofibrils
164 (Fig. 2B,D; Fig. S2). In late third instars, the sarcomeric pattern was disrupted almost entirely on
165 the visceral side of anterior segments and large bundles of F-actin replaced organized myofibrils
166 (Fig. 2C,F; Fig. S2). Occasionally, interlaced “braided” myofibrils formed at the beginning of late
167 third instar, and ectopic radial F-actin accumulations arose by the end of late third instar (Fig.
168 2E,G). Additionally, once the first diagonally misoriented myofibrils were observed, perpendicular
169 myofibrils were found adjacent to the myotendinous junction (MTJ) at the posterior myofiber end
170 (Fig. 2B). These perpendicular myofibrils also later developed at the anterior end of the myofibers
171 (Fig. 2C). Nuclear irregularities appeared in anterior segments during late third instar stage and,
172 together with ectopic F-actin structures, were only observed in anterior segments. These data
173 indicated Tmod-KD myofibers experience a specific temporal and spatial pattern of structural
174 changes, which appeared in parallel with larval growth, with the most severe disruptions occurring
175 in dramatically growing third instar larvae.
176
177 **Tmod’s role as a pointed-end capping protein is conserved in *Drosophila***
178 To understand how Tmod loss generates these phenotypes, we studied the biochemical activity
179 of *Drosophila* Tmod using purified proteins *in vitro*. Tmod’s canonical role in vertebrates is filament
180 pointed-end capping (Dye et al., 1998, Weber et al., 1994, Gregorio et al., 1995, Mardahl-
181 Dumesnil and Fowler, 2001, Fowler and Dominguez, 2017). However, some Tmods also have
182 limited actin filament nucleation activity (Fischer et al., 2006, Yamashiro et al., 2010, Yamashiro
183 et al., 2014), mimicking the activity of Tmod’s structural homolog Lmod that has strong nucleation

184 activity (Chereau et al., 2008). Lmod is not found in *Drosophila*. Nonetheless, while mammals
185 express only four Tmod isoforms, *Drosophila* expresses 18 different splice variants. Moreover,
186 several *Drosophila* Tmod isoforms differ substantially in sequence from their mammalian
187 counterparts, displaying N- and/or C-terminal extensions reminiscent of those present in
188 mammalian Lmods (Fig. S3F). These observations led us to ask whether *Drosophila* Tmod
189 isoforms capped pointed-ends or nucleated filaments.
190
191 We chose two isoforms for *in vitro* analysis, the selection of which was based on several criteria:
192 the RNAi target sites, the abundance of the transcript in control muscle, the degree of KD,
193 sequence analysis, and the unique structures of the isoforms (Fig. S3A-F, Table S3). Based on
194 these factors, isoforms Q, O, and K, representing two different N-terminal subgroups, were
195 chosen for in-depth biochemical analysis (note that isoforms O and K have identical protein
196 sequences). We expressed and purified TmodQ, TmodO/K, and human TMOD3 (a control for
197 capping activity) in *E. coli* and monitored the effect of TmodQ and TmodO/K on actin assembly
198 using the pyrene-actin polymerization assay (Doolittle et al., 2013). Because the concentration of
199 actin monomers (1.5 μM) is higher than the critical concentration for monomer addition at the
200 pointed-end (~0.6 μM), pointed-end capping under these conditions would be observed as a
201 decrease in fluorescence with increasing Tmod concentrations, resulting from inhibition of
202 monomer addition at the pointed-end. In contrast, if Tmod nucleated filaments from monomers
203 we would observe an increase in fluorescence (i.e. polymerization), resulting from the formation
204 and elongation of new barbed-ends. Similar to human TMOD3, TmodQ and TmodO/K reduced
205 polymerization in a concentration-dependent manner (Fig. 3A; Fig. S3G,H). These results
206 suggested that the two representative *Drosophila* Tmod isoforms analyzed function as *bona fide*
207 pointed-end cappers like their mammalian Tmods, and not nucleators like mammalian Lmods.
208 Therefore, the observed KD phenotypes are likely due to a deficiency in pointed-end capping.
209
210 **Tmod regulates thin filament and sarcomere length**
211 Previous work has shown that Tmod regulates sarcomere length by capping the pointed-end of
212 sarcomeric F-actin [reviewed in Littlefield and Fowler (2008), Ghosh and Fowler (2021)]. To
213 assess the effects of Tmod-KD in *Drosophila* larval myofibers, we quantified muscle length, Z-
214 disc number, and sarcomere lengths in second and late third instars. At both timepoints, Tmod-
215 KD myofibers had fewer Z-discs than controls with the same length (Fig. 3D; Fig. S4A,B). Z-disc
216 numbers were reduced by 15% in the second instar and by 26% in late third instar, indicating that
217 sarcomere size increased in growing Tmod-KD myofibers. Accordingly, the distance between Z-

218 discs revealed a significant 22% and 31% increase in sarcomere length in Tmod-KD myofibers at
219 the second and late third instar stages, respectively (Fig. 3C). To confirm that Tmod regulates
220 sarcomere size via its effect on thin filaments, we quantified sarcomeric F-actin length in late third
221 instars. Thin filament length increased by 35% in Tmod-KD myofibers. Interestingly, the proportion
222 of thin filament length to sarcomere length was similar to control, whereby thin filaments account
223 for 25% of sarcomere length (Fig. 3B,F). Together, these data suggested that capping of
224 sarcomeric F-actin by Tmod is required to prevent increases in sarcomere size during myofiber
225 growth. The same thin filament to sarcomere length ratio in Tmod-KD and control myofibers
226 indicates that independent mechanisms maintain sarcomere proportions.
227
228 Sarcomere size is highly conserved for optimal contraction, and changes in its size have been
229 linked to reduced muscle function (Fernandes and Schock, 2014, Molnar et al., 2014, Spletter et
230 al., 2018, Spletter et al., 2015). To assess the functional consequences of muscle-specific Tmod
231 KD, we performed larval locomotion assays. We analyzed larval velocity throughout larval
232 development and myofiber function significantly decreased, starting at second instar stage and
233 over larval development (Fig. 3E). These data suggested Tmod-KD caused myofiber weakness
234 even before obvious muscle deterioration, and that changes in thin filament length could be the
235 first effect of Tmod KD to reduce muscle function.
236
237 **Tmod stabilizes core components of the muscle attachment site**
238 The current model of myofibrillogenesis suggests that tension is crucial for this process.
239 Specifically, the muscle attachment sites at the MTJs play a fundamental role in generating
240 tension within a myofiber. The MTJ represents an analogous structure to focal adhesion sites
241 (Atherton et al., 2016, Martino et al., 2018, Pardo et al., 1983, Quach and Rando, 2006,
242 Mohammad et al., 2012), which are composed of the Vinculin-Talin-Integrin complex tethering the
243 actin cytoskeleton to the ECM, or in the case of the myofiber, the myofibrils to the muscle
244 attachment site. We hypothesized that Tmod functions at the MTJs to stabilize myofibril
245 attachment during myofiber growth.
246
247 In agreement with this hypothesis, we detected Tmod localized at the ends of control myofibers,
248 adjacent to myofibrillar F-actin and co-localizing with β_{PS}-Integrin (Mys) (Fig. 4A,C). We next
249 evaluated protein enrichment of the tension-mediating proteins β_{PS}-Integrin and its binding partner
250 Talin (Rhea) in Tmod-KD MTJs. β_{PS}-Integrin and Talin were significantly decreased in Tmod-KD
251 anterior segments (Fig. 4E,F; Fig. S5A-C), however we did not detect myofiber detachment. To

252 determine whether the strong decrease in signal was due to mislocalization or an overall decrease
253 in protein levels, we performed Western blot analysis. Talin levels did not decrease in Tmod-KD
254 wandering larvae muscle-enriched lysates (Fig. 4B), suggesting that Talin is mislocalized. Upon
255 further examination, we observed pools of β_{PS}-Integrin and Talin in ectopic areas (Fig. 4F). These
256 data suggested Tmod's F-actin capping function is required for establishing the proper anchorage
257 sites at the myofiber ends by stabilizing the interaction between F-actin and tension-mediating
258 proteins.
259
260 To address whether mislocalization of β_{PS}-Integrin and Talin correlated with tension loss at the
261 MTJ, we assessed phospho-tyrosine (pTyr), a marker of active cytoskeletal tension sites
262 (Chrzanowska-Wodnicka and Burridge, 1994, Martino et al., 2018, Parsons et al., 2010). pTyr
263 was significantly decreased in Tmod-KD MTJs (Fig. 4F; Fig. S5D), indicating reduced tension.
264 Together, these experiments suggested a decrease in mechansensory proteins and a reduction
265 of tension at the muscle ends. A lack of tension could cause myofibrillar disorganization and
266 impaired myofibrillogenesis in the Tmod-KD myofibers.
267
268 **Tmod regulates myonuclear morphology, positioning, and function**
269 Cytoplasmic F-actin is found in and around the nucleus (Davidson and Cadot, 2021, Caridi et al.,
270 2019). These filaments play roles in gene expression, in the cell's response to mechanical stimuli,
271 and in nuclear positioning in several systems (Farina et al., 2016, Verheyen and Cooley, 1994,
272 Chang et al., 2015). We hypothesized Tmod-KD could affect cytoplasmic F-actin to generate the
273 nuclear phenotypes that we observed. Control *Drosophila* larvae displayed multiple, evenly
274 spaced, round disc-shaped nuclei on the myofiber's visceral side. In contrast, many Tmod-KD
275 nuclei were elongated, with an increased perimeter compared to control (Fig. 5A-C). Along the
276 AP axis, the most irregular-shaped nuclei were located towards the middle of the myofiber (Fig.
277 5D). It is possible Tmod-KD directly affected F-actin dynamics that stabilize nuclear shape and
278 position. Unfortunately, imaging of cytoplasmic and/or nuclear F-actin is obstructed by the bright
279 signal of the underlying sarcomeres, which prevented the further analysis of direct effects of
280 Tmod-KD on cytoskeleton and nucleoskeleton in this study.
281
282 Stable radial microtubule (MT) arrays around the nuclei maintain positioning and nuclear integrity
283 during myofiber contraction (Zheng et al., 2020, Becker et al., 2020, Manhart et al., 2018, Metzger
284 et al., 2012). In addition, MTs physically interact with actin (Farina et al., 2016, Dogterom and
285 Koenderink, 2019), which raises the possibility that actin-MT crosstalk supports nuclear shape

286 and position. To assess if perinuclear MTs were affected in Tmod-KD muscles, we quantified the
287 number of intact radial MT arrays in control and Tmod-KD myofibers. We observed a significant
288 decrease in intact perinuclear MT arrays in Tmod-KD muscles and noted a decrease in
289 longitudinal MT-tracks (Fig. 5E; Fig. S6A). These data indicated that Tmod affects critical MT
290 networks in myofibers, by mediating the interactions of the MT cytoskeleton with actin filaments
291 in/around the nuclei. A loss of perinuclear MTs could subsequently result in destabilization of
292 nuclear shape and position.
293
294 To test if nuclear activity was affected by nuclear morphology, we analyzed the transcriptional
295 and translational potential of Tmod-KD myonuclei. To assess transcription, we quantified H3K9ac,
296 a marker of open chromatin and transcriptionally active regions in the DNA (Kharchenko et al.,
297 2011). Nuclei with the most irregular shapes (roundness<0.6) exhibited decreased H3K9ac levels,
298 whereas WT-shaped nuclei (roundness>0.6) showed similar H3K9ac levels to control (Fig. 5F,H;
299 Fig. S6B). To assess translation, we quantified nuclear intensity of Fibrillarin (Fib), a nucleolar
300 protein that plays an essential role in ribosome biogenesis and is a commonly used readout for
301 protein synthetic ability (Gillery et al., 1996, Lefevre et al., 2001). Misshaped nuclei
302 (roundness<0.6) exhibited similar Fib intensity levels to control, while WT-shaped nuclei
303 (roundness>0.6) showed higher levels than control (Fig. 5G,I; Fig. S6C). These data suggested
304 that loss of nuclear shape and position in Tmod-KD myofibers reduced transcriptional output but
305 increased translational potential. While deformed nuclei are functionally compromised, WT-
306 shaped nuclei in the Tmod-KD muscle appeared to compensate for this deficiency by increasing
307 translation.
308
309 **Tmod knockdown alters actin isoforms, degradation, and oxidative metabolism**
310 We analyzed the transcriptome of Tmod-KD larvae to better understand the mechanisms behind
311 the observed phenotypes and uncover additional consequences. Consistent with the
312 morphological features found in Tmod-KD muscle, we detected misregulation of actin genes.
313 Sarcomeric actin isoforms (Act57B, Act87B) (Roper et al., 2005, Fyrberg et al., 1983) were
314 upregulated (Fig. 6; Table S4), consistent with the observed ectopic F-actin bundles (Fig. 2F-G;
315 Fig. 6E). In contrast, cytoplasmic actin isoforms (Act5C, Act42A) were downregulated in Tmod-
316 KD myofibers (Fig. 6E; Table S4), consistent with the alterations in nuclear shape detected in
317 Tmod-KD.
318

319 We also performed an over-representation analysis (ORA) to determine if a set of shared genes
320 was differentially expressed based on Gene Onthology (GO) and Kyoto Encyclopedia of Genes
321 and Genomes (KEGG) gene sets. These data indicated that degradation-related genes
322 (particularly proteasomal genes) and/or pathways were downregulated, while metabolism-linked
323 genes (particularly oxidative metabolism genes linked to mitochondrial ATP production) and/or
324 pathways were upregulated in Tmod-KD muscles (Fig. 6A,B). To test whether ATP production
325 was indeed altered in Tmod-KD muscles, we performed a functional ATPase assay. Consistent
326 with our RNAseq data, ATP levels significantly increased in Tmod-KD myofibers (Fig. 6C).
327 Together, these data suggested a role for Tmod, either directly or indirectly, in gene expression.
328 We speculate that these changes reflect a compensatory mechanism to promote growth in a
329 degenerating muscle.
330
331

332 **DISCUSSION**

333 Tmod function has been studied using various cell types (Fowler, 1997). Here we investigated
334 the effects of Tmod KD in *Drosophila* larval myofibers during development using a combination
335 of detailed *in vivo* analyses, *in vitro* experiments, and transcriptomic approaches. Our studies
336 suggest that through its capping function, Tmod affects actin dynamics in different locations within
337 the myofiber and is ultimately essential for muscle function.

338

339 We propose the following model for Tmod's pleiotropic effects in muscle cells (Fig. 7). In the
340 sarcomere, the barbed end of F-actin is capped by CapZ and anchored to the Z-disc, while the
341 pointed-end is capped by Tmod. However, due to Tmod's low affinity for F-actin (Weber et al.,
342 1994), there are yet opportunities for monomer addition and therefore, the pointed-end remains
343 suitable for sarcomere growth. When Tmod is knocked-down, thin filaments grow in length. We
344 suggest this additional polymerization causes sufficient imbalance to favor the production of
345 muscle-specific larval G-actin isoforms (Act57B, Act 87E); this increased G-actin availability and
346 continuously growing sarcomeric F-actin would result in ectopic F-actin bundles and radial
347 structures. In the cytoplasm, F-actin growth occurs through the canonical pathway, which is,
348 generally, by the addition of G-actin monomers at the barbed end and depolymerization at the
349 pointed-end. When Tmod is reduced, excessive depolymerization occurs, due to loss of Tmod's
350 capping activity. This excess of G-actin monomers decreases the production of cytoplasmic-
351 specific actin isoforms (Act5C, Act42A). Loss of cytoplasmic perinuclear and nuclear F-actin
352 would contribute to the loss of nuclear organization and directly or indirectly affect nuclear output.
353 At the MTJ, myofibrils are anchored to the muscle ends via cytoplasmic F-actin. In the absence
354 of Tmod, lack of stable attachments via F-actin impairs tension along the myofibrils, leading to
355 myofibril disorganization and deterioration, and defects in myofibrillogenesis. Protein degradation
356 and metabolism would be affected similarly by destabilization of required structures for myofiber
357 organization or via transcriptional changes. Together, loss of Tmod at these different sites leads
358 to impaired muscle function.

359

360 While every myofiber experiences the same Tmod-KD effect and follows the same pattern of
361 deterioration, not every myofiber is affected equally. Along the larval AP axis, we see that the
362 *tmod* phenotypes appear first and are most severe in anterior abdominal segments which contain
363 larger muscles than posterior segments, suggesting that growth and/or myofiber size may be a
364 contributing factor. However, we observe that some muscles at the same axis position are
365 preferentially affected, which suggests a more complex situation. Freely moving *Drosophila* larvae

366 constantly pivot and sweep their heads, which are supported by muscles of segments A1-A3
367 (Lahiri et al., 2011); hence, muscle usage may affect muscle deterioration in our model. In parallel,
368 the timing and distribution of muscle pathology in many human muscle diseases, as well as animal
369 models, follow specific patterns (Barohn et al., 2014, Sewry et al., 2019). Studies in vertebrate
370 models suggest that muscle fiber type might play a role [reviewed in Talbot and Maves (2016)].
371 The factor(s) that make specific muscles more susceptible to deterioration remain unknown. The
372 *Drosophila* larval musculature, consisting only of one fiber type, provides a useful system for
373 further studies in this context.
374
375 Alternative splicing results in a total of 18 Tmod isoforms. Why the fly produces so many different
376 isoforms is unclear. We show that isoforms Q and O/K display Tmod's characteristic F-actin
377 capping function, despite having N-terminal extensions comparable to human LMOD. We did not
378 find biochemical evidence of F-actin nucleation. It is possible that one of the remaining Tmod
379 isoforms (most notably the isoforms with C-terminal proline-rich extensions) may possess
380 nucleation activity like that of human LMODs. However, the extremely low levels of such isoforms
381 in our RNAseq data suggest they are not expressed in myofibers, or at the tested developmental
382 stages.
383
384 Tmod is suggested to define thin filament and sarcomere length in a variety of model systems
385 (Szikora et al., 2022). In adult *Drosophila*, Tmod overexpression results in shorter sarcomeres
386 and thin filaments (Molnar et al., 2014, Mardahl-Dumesnil and Fowler, 2001). In vertebrate
387 systems, such as mouse Tmod-null mutants, thin filament length increases (Littlefield and Fowler,
388 2008). *In vitro* rat cardiomyocytes show increased or decreased Tmod levels resulting in shorter
389 or longer sarcomeric actin filaments, respectively (Sussman et al., 1998). Our data demonstrate
390 that Tmod-KD in *Drosophila* larval myofibers increases thin filament and sarcomere length. Thin
391 filament to sarcomere length ratio was maintained in Tmod-KD myofibers. This ratio was similar
392 to measurements in frog sartorius (26%) and human pectorialis (30%) (Gokhin and Fowler, 2013).
393 This indicates that mechanisms that regulate sarcomere proportions are conserved and regulated
394 independently of Tmod function. We further find sarcomere size increases throughout larval
395 growth, indicating that the uncapped pointed-ends of sarcomeric actin filaments do not respect a
396 specified size, exhibiting continuous polymerization in Tmod's absence. In healthy muscle,
397 sarcomere length is fixed to optimize muscle contraction, forcing growing cells to add sarcomeres
398 rather than increasing their length (Balakrishnan et al., 2020, Williams and Goldspink, 1971, Dix
399 and Eisenberg, 1990, Goldspink, 1983, Haas, 1950). We show an inverse relationship between

400 sarcomere number and length in Tmod-KD myofibers, suggesting that myofibrils could grow by
401 increasing their length via sarcomere growth. Consistent with recently published work, our data
402 indicates that muscle length and sarcomere number are regulated independently of one another
403 (Brooks et al., 2022). Loss of this adaptive behavior is associated with myopathy progression
404 (Ottenheijm et al., 2009, Winter et al., 2016). Moreover, the decrease in myofiber size is
405 suggestive of compromised myofibril addition to increase muscle mass, which further supports
406 that mechanisms of muscle growth (addition of new sarcomeres and hypertrophy) are affected in
407 Tmod-KD larvae. Our analyses show locomotive defects (first instar) before discernable changes
408 in myofiber structure (second instar). While technical limitations prevented the detailed analysis
409 of first instar sarcomeres, we suggest that changes in thin filament length might be the first effects
410 of Tmod KD that directly affect muscle function. In parallel with disruption of sarcomeres and
411 myofibrils, Tmod-KD myofibers display accumulation of ectopic and disorganized F-actin. The
412 location of these ectopic bundled and radial F-actin accumulations near disorganized myofibrils
413 indicates that continuously growing thin filaments could contribute to these ectopic structures.
414 Whether the ectopic disorganized F-actin filaments were intended to serve as a myofibril template
415 (Fenix et al., 2018, Dlugosz et al., 1984) or they result from deteriorating myofibrils remains
416 unclear.
417
418 The currently favored hypothesis in the field describes sarcomere and myofibril formation as a
419 tension-driven self-organizing process, whereby tension generated through muscle attachment at
420 the MTJs is used to orient and longitudinally assemble sarcomeres and myofibrils (Lemke and
421 Schnorrer, 2017). Here, we show that Tmod-KD results in mislocalization of two core
422 mechanosensitive proteins and a reduction in tension at the muscle ends. According to the
423 hypothesis, lack of tension at the muscle ends affects addition of new sarcomeres as well as
424 homeostasis along the entire myofibril. This is consistent with our Tmod-KD data showing reduced
425 sarcomere number and aberrant myofibril organization and stability. Previous studies using *tmod*
426 mutant zebrafish also reported defects in myofibril organization and muscle weakness (Berger et
427 al., 2022, Berger et al., 2014), but a role for Tmod in sarcomere addition had not been described.
428 Interestingly, we observe perpendicular myofibrils exclusively localized at the myofiber ends,
429 which demonstrate sarcomeric organization albeit incorrect orientation. This raises the possibility
430 that due to the lack of longitudinal stability in this growth zone, the forming sarcomeres and
431 growing myofibrils orient towards the next best structure that provides resistance, connecting to
432 the MTJ, existing myofibrils or the visceral plasma membrane. A similar phenotype with
433 misoriented myofibrils was observed in *Drosophila* larval muscle expressing the constitutively

434 active form of C3G, a Rap1 activator (Shirinian et al., 2010). Importantly, Rap1 has been
435 demonstrated to recruit Talin to the cell membrane (Shattil et al., 2010, Lee et al., 2009). We find
436 ectopic localization of mechanosensitive proteins along the plasma membrane of Tmod-KD
437 myofibers, which could lead to ectopic F-actin accumulations. This could result in local changes
438 in tension throughout the myofiber and contribute to myofibril misalignment. Together, our study
439 suggests that Tmod is crucial for maintaining alignment, stability, and growth of myofibrils. Our
440 data are consistent with the tension-driven self-organizing myofibrillogenesis hypothesis and adds
441 a role for Tmod in tension mediation.
442
443 Our data implicates Tmod in nuclear positioning in the Z-axis and maintaining nuclear
444 morphology. Mispositioned and deformed nuclei are common in many myopathies and
445 laminopathies (Romero, 2010, Steele-Stallard et al., 2018, Ross et al., 2019), highlighting the
446 relevance of correct nuclear positioning for proper muscle function. Actin plays a structural role in
447 the nucleus (Bettinger et al., 2004); hence Tmod, through its capping function, may stabilize nuclear
448 and/or perinuclear actin to directly support nuclear integrity. We did not detect nuclear or
449 perinuclear actin filaments, possibly due to the strong F-actin signal of the adjacent thin filaments.
450 However, we found defects in the MT networks surrounding the nuclei of Tmod-KD myofibers.
451 MTs interact with actin filaments and are crucial in myonuclear positioning and integrity. Thus,
452 Tmod-KD likely has indirect effects on myonuclei by disrupting actin-MT interactions. In addition,
453 defects in nuclear positioning and morphology could be indirectly affected by the loss myofibril
454 structure and orientation. In Tmod-KD myofibers, nuclei are initially located at the periphery, but
455 subsequently sink as myofibril structure is lost. Force exertion on the internalized nuclei could
456 then lead to deformation of nuclear shape. These nuclei also show defects in transcriptional
457 activity. Interestingly, WT-shaped nuclei in Tmod-KD myofibers display increased translation makers,
458 consistent with a compensatory mechanism. In addition to the effects of nuclear morphology, it is
459 possible that Tmod regulates transcription and/or translation via its effect on actin dynamics. G-actin
460 has many important functions in the nucleus and nucleolus and directly regulates gene transcription
461 (Visa and Percipalle, 2010, Bettinger et al., 2004). More research is needed to determine how
462 deviation from normal positioning in 3 dimensions (X,Y,Z) results in impaired muscle function. To
463 this end, future studies focused on the distribution of gene products throughout the myofiber when
464 nuclear positioning is aberrant would be informative.
465
466 Our transcriptome analyses suggest that Tmod KD affects two main processes, proteasomal
467 degradation and mitochondrial metabolism, both critical for myofiber growth (Schiaffino et al.,

468 2013). However, the decrease in degradation and increase in mitochondrial metabolism detected
469 in Tmod-KD myofibrils is inconsistent with the observed impaired muscle growth and muscle
470 weakness. We suggest that this transcriptomic profile indicates a compensatory attempt of the
471 myofibers to grow, counteracting the lack of tension along the myofiber and structural
472 deterioration. It is possible that actin inside the nucleus causes these changes through structural
473 and/or transcriptional changes (Chase et al., 2013, Visa and Percipalle, 2010). However, similar
474 myofiber phenotypes and changes in metabolism have been observed in *Drosophila TRIM32*
475 (*thin*) mutant larval muscles (LaBeau-DiMenna et al., 2012, Bawa et al., 2020). Loss of *Drosophila*
476 TRIM32*,* an E3-ubiquitin ligase, resulted in a decrease in glycolytic intermediates, indicating that
477 TRIM32 switches metabolism from oxidative to glycolytic. The mechanisms by which TRIM32 and
478 Tmod are connected remain to be elucidated, yet the similarities in phenotype and transcriptome
479 suggest they might be interacting genetically or biochemically. This would indicate a role for Tmod
480 in dampening oxidative metabolism and, therefore, ATP production. Strikingly, structural
481 components involved in these pathways, such as mitochondria, are located in high densities at
482 the visceral muscle surface and around myofibrils; hence, they could be affected indirectly via the
483 destabilization of the underlying myofibrils.
484
485 Myopathies are often devastating disorders characterized by impaired muscle function that are
486 frequently associated with sarcomeric mutations. The molecular details underpinning this
487 relationship are poorly understood. Our study shows a series of phenotypes associated with KD
488 of one critical thin filament component, Tmod, that reach far beyond the sarcomere. Our findings
489 have important implications, as they suggest a key role for Tmod in several cellular processes,
490 including the regulation of actin isoform expression, the stabilization of tension-mediating proteins,
491 and nuclear integrity and positioning, therefore providing additional insight to the pathogenesis of
492 myopathies. The mechanisms directly linking Tmod and critical myofiber processes, including
493 proteasomal degradation and oxidative metabolism, remain to be fleshed out. Furthermore, our
494 findings support and strengthen the tension-driven self-organizing myofibrillogenesis model.
495 Taken together, this study adds significantly to the understanding of Tmod in muscle
496 development, maintenance, and disease, making it a potential target for new therapeutics that
497 address muscle weakness.
498

499 **METHODS**

500 ***Drosophila* husbandry, stocks and crosses**

501 *Drosophila* stocks and experimental crosses were grown on standard cornmeal medium at 25ºC
502 in 12:12 Light:Dark conditions under humidity control. The Gal4-UAS system (Brand and
503 Perrimon, 1993) was used for RNA interference studies. Details on the screen that lead to our
504 analysis of *tmod* are found in Table S1 and S2. For muscle-specific expression and RNAi
505 potentiation we tested different driver lines (*UAS-dicer2;;Mhc-Gal4,Zasp66::GFP*, *UAS-*
506 *dicer2;;Dmef2-Gal4,Zasp66::GFP/Tm6,Hu,Tb* and *UAS-dicer2;;Dmef2-Gal4/Tm6,Hu,Tb*) in
507 combination with *3 UAS-tmod-RNAi* lines (BDSC#41718, BDSC #31534 and VDRC #108389) to
508 validate on-target effects and explore KD levels. The driver lines were crossed with *UAS-*
509 *mCherryRNAi* (BDSC #35785) as the *control RNAi.* In all instances, larvae displaying a Tb
510 phenotype (indicatory of balancer chromosome) were excluded from the F_1 analyzed. The mutant
511 stock $tmod^{MI02468}$ (BDSC #36446) was also used for phenotype validation with *yw* as control.
512 Except where specified, we used a Dmef2-Gal4 driver and one *UAS-tmodRNAi* line
513 (BDSC#41718) for analyzing Tmod-KD phenotypes (the line is referred to as "*tmod"*). Table S5
514 contains details on fly stocks.

515

516 **Larval staging**

517 For all larval experiments, larvae were kept at 25ºC and both male and female larvae were
518 analyzed. Staging was performed on apple juice agar plates, either in the embryo (see Viability
519 assay), or by selecting larvae hatched within a 2h period. First instars intended for experiments
520 were maintained in an apple juice agar plate with yeast paste for ease of manipulation. Larvae for
521 experiments at later stages (locomotion, muscle analysis) were transferred to standard food vials.
522 Larvae were removed from food vials using 30% sucrose solution at second instar stage (~24h
523 after transfer), early third instar (~48h after transfer), late third instar (~96h after transfer) and
524 wandering (~118h after transfer) stage. Myofiber structure time-course analysis was performed
525 on all four distinct larval stages, in VI1 or VL3/VL4 muscles of anterior segments (A1 and A2). For
526 the RNAseq experiment, late third instars (~90h after transfer) were processed for dissection. For
527 all other experiments at late third instar stage (~3.5 days), staging was confirmed by using
528 developmental landmarks such as mouth hooks, and spiracle morphologies (Bodenstein, 1950).

529

530 **qRT-PCR**

531 Ten third instar wandering larvae were dissected and rinsed in ice cold HL3.1 medium (Feng et
532 al., 2004) as described in (Brent et al., 2009). Total RNA was extracted from the muscle enriched

533 larval fillets using TRIzol reagent (ThermoFisher #15596026), followed by cleanup with TURBO
534 DNA-free Kit (Ambion #AM1907). The SuperScript III First-Strand Synthesis System for RT-PCR
535 (Invitrogen #18080-051) was used to synthesize cDNA and qRT-PCR reactions were performed
536 on the BioRad CFX96 Real-Time PCR system using the SYBR Select Master Mix for CFX
537 (Applied Biosystems #4472937). Three independent mRNA preparations per genotype were
538 collected and were run in triplicate. Fold changes were calculated based on values obtained using
539 the delta-delta Ct method (Livak and Schmittgen, 2001, Schmittgen and Livak, 2008). Product
540 size and uniformity was assessed via melt curve analysis. *Rpl32* was used as a normalization
541 control. Table S3 contains details on the oligonucleotides used.
542
543 **Western Blot**
544 Seven to ten late third instar wandering larvae were dissected (See Immunolabeling and Imaging)
545 and transferred into larval lysis buffer (50mM HEPES pH 7.5, 150mM NaCl, 0.5% NP40, 0.1%
546 SDS, 2mM DTT) supplemented with Complete mini protease inhibitor cocktail [one tablet in 10mL
547 of lysis buffer (Roche #11836153001)]. Lysates were homogenized and protein concentrations
548 were determined using the Bradford assay. Equal amounts of protein (20 μg) were run on a 5%
549 (Talin) or 10% (Tmod) polyacrylamide gel and then transferred onto a nitrocellulose membrane
550 (ThermoScientific #88018). Membranes were blocked with either 5% milk or 5% BSA in TBST
551 (Tris-Buffered Saline +0.1% Tween) for 1h at room temperature. Table S5 contains details on
552 primary and secondary antibodies. Immunoreactions were visualized in a KwikQuant Imager
553 (Kindle Biosciences, LLC #D1001) using 1-Shot Digital-ECL (Kindle Biosciences, LLC #R1003)
554 and intensities were quantified using Fiji (NIH). Protein expression was normalized to GAPDH
555 (loading control) within each sample. Figures and quantifications are representative of 3
556 experiments.
557
558 **Larval tracking**
559 Larvae were staged and extracted from food vials (see Larval staging) at first instar, second instar,
560 early third instar, and late third instar. One larva at a time was placed at the center of an apple
561 juice agar plate (8.5cm diameter) and recorded for 45 seconds (Samsung Galaxy S8+). Movies
562 were converted into image sequences (1 image per second) and each larva was tracked using
563 the Manual Tracking plug-in on Fiji. Average velocity was calculated as in (Balakrishnan et al.,
564 2021). For each genotype, we performed three replicates with ~10 larvae each. Larval length was
565 equivalent in both phenotypes for each developmental stage.
566

567 **Plasmids**

568 The cDNA for TmodO/K (NCBI Reference Sequences: NP_001247373.1 / NP_001189319.1) was
569 acquired from DNAsu clone DmCD00765633 (Tempe, AZ, USA). The cDNA for TmodQ (NCBI
570 Reference Sequence: NP_001263112.1) was synthesized by GeneWiz (South Plainfield, NJ,
571 USA). Each cDNA was PCR-amplified and ligated between the SacI and KpnI sites of
572 pRSF_Duet1 (Millipore Sigma, Burlington, MA, USA) with an N-terminal 6x histidine tag and a C-
573 terminal Strep-II tag.

574

575 **Protein expression and purification**

576 Tmod isoforms in pRSF_Duet1 were expressed in ArcticExpress(DE3) RIL cells (Agilent
577 Technologies), grown in Terrific Broth (TB) medium for 6 h at 37 °C to an optical density of ~1.5
578 at 600 nm (OD600), followed by 24 h at 10°C in with 0.4 mM isopropyl-β-D-thiogalactoside (IPTG).
579 Cells were harvested by centrifugation (4,000g), resuspended in nickel buffer (20 mM HEPES pH
580 7.5, 300 mM NaCl, 10 mM imidazole, 1 mM PMSF), and lysed using a microfluidizer apparatus
581 (Microfluidics). Proteins were first purified on nickel-NTA resin, washed with 20 column volumes
582 of nickel buffer, and eluted using nickel buffer supplemented with 300mM imidazole. Elution
583 fractions containing the Tmod proteins were then loaded onto Streptactin XT resin (IBA Life
584 Sciences, Göttingen, Germany) and washed with 20 column volumes of strep buffer (20 mM
585 HEPES pH 7.5, 150 mM NaCl, 1 mM EDTA). Proteins were eluted using strep buffer
586 supplemented with 40mM biotin, and further purified through a SD200HL 26/600 gel filtration
587 column (GE Healthcare) in strep buffer supplemented with 1 mM DTT. Human CapZ (Rao et al.,
588 2014), rabbit skeletal muscle actin (Pardee et al., 1982), and rabbit skeletal muscle tropomyosin
589 (Smillie, 1982) were purified as described.

590

591 **Pointed-end capping assay**

592 Capping assays were carried out as described previously (Rao et al., 2014, Kumari et al., 2020).
593 Briefly, 1.5 μM of pre-formed F-actin seeds, coated with 1 μM Tropomyosin and capped at the
594 barbed end with saturating amounts of CapZ (25 nM), were incubated and assayed alone or with
595 4 different concentrations (25, 100, 400, 800 nM). Upon addition of 1.5 μM G-actin (6% pyrene-
596 labeled), reactions were monitored as the fluorescence increase resulting from the incorporation
597 of pyrene-actin monomers at the pointed-end. Pyrene fluorescence (excitation 365 nm, emission
598 407 nm) was detected using a plate reader (BioTek Cytation 5), and for each Tmod concentration
599 four replicates were recorded. Maximum polymerization rates were determined by taking the first

600 derivative of each curve, identifying the time interval corresponding to the greatest slope, and
601 performing a linear regression on the original data within that time interval.
602
603 **Immunostaining and confocal imaging**
604 Larvae were dissected in ice cold HL3.1 medium as described in (Brent et al., 2009) and fixed
605 with 10% formalin (Sigma-Aldrich #HT501128) for 20 minutes. Larval filets were blocked with
606 PBT-BSA [1x PBS supplemented with 0.3% Triton X-100 (Sigma-Aldrich #X100) and 0.1% BSA
607 (Sigma-Aldrich #A7906)] for 30 minutes. Larval filets were then incubated with primary antibody
608 (Table S5) overnight at 4ºC, followed by washes in PBT-BSA. Incubation with Alexa Fluor-
609 conjugated secondary antibodies (Table S5), Phalloidin and/or Hoechst 3342 were performed at
610 room temperature for 2 hours, followed by washes in PBT. Subsequently, larval filets were
611 mounted in ProLong Gold (Invitrogen #P36930) and slides were cured at room temperature for
612 24h. Z-stacks were acquired using a SP5 laser-scanning microscope (Leica Microsystems) with
613 either dry objectives (HC PL APO CS 10x/0.40 and HC PL APO CS2 20x/0.75) or oil-immersion
614 objectives (HC PL APO CS 20x/0.70, HCX PL APO CS 40x/1.25-0.75, HCX PL APO CS 63x/1.40-
615 0.60, and HCX PL APO CS 100x/1.46). All samples intended for direct comparison were imaged
616 using the same confocal settings. Maximum intensity projections of confocal Z stacks were
617 rendered using Fiji. Approximately 7 larvae (range: 5-10) of each genotype were dissected and
618 experiments were repeated at least twice.
619
620 **Quantification of muscle defects per segment**
621 Muscle defects in second instar, early third instar, and late third instar larvae were scored based
622 on ectopic and abnormal actin structures using a confocal microscope. A score was given for
623 each VL3/4 muscle pair: 3 – WT-like, 2 – mild structural defects (diagonal myofibrils) and 1 –
624 severe defects in muscle structure. We evaluated muscles in both hemisegments of the larva in
625 abdominal segments 1-6. This analysis was performed in triplicate with 3-4 larvae per replicate.
626
627 **Sarcomere and thin filament size/count analysis**
628 Larvae expressing a Zasp::GFP protein trap were fixed by brief (~5 seconds) submersion in 65°C
629 water and mounted on a slide with halocarbon oil. Z-stacks of the cuticular side of the VL3 or VL4
630 muscles from abdominal segment 2 were acquired using a SP5 laser-scanning microscope (Leica
631 Microsystems) with either a HC PL APO CS2 20x/0.75 (late third instars) or HCX PL APO CS
632 40x/1.25-0.75 (second instars) oil immersion objective.
633

634 Muscle length, sarcomere size and number were quantified as described in step 32 of
635 (Balakrishnan et al., 2021). For accuracy and to assess potential regional differences, sarcomere
636 size was also quantified by an alternative method. Z-stacks were opened in Fiji and a line that
637 spanned six Z-discs (five sarcomeres) was made using the line tool. Subsequently, the line
638 intensity plot was obtained, and the X-coordinates (microns) of the peaks were acquired with the
639 multi-point tool. The distance in microns between Z-disks was obtained by calculating the
640 difference between the X-coordinates of the six peaks. This analysis was done in triplicate. In
641 each replicate, six muscles were analyzed, each belonging to an individual larva. Three lines were
642 traced per muscle: in the anterior fraction of the muscle, in the medial region and in the posterior
643 end, with a total of ~90 sarcomere size measurements per replicate (Fig. S4C).
644
645 Sarcomere length was obtained from Zasp::GFP heat-fixed larvae, which was performed by a
646 direct method from Z-disc to Z-disc distance. Due to technical challenges in some areas of the
647 muscles, two confirmatory methods were also employed. First, measurements were confirmed by
648 comparing the heat-fixed samples with a formalin fixed sample. Second, we performed a
649 sarcomere length average by taking the muscle length divided by the total number of Z-discs.
650
651 Thin filament length was assessed in formalin fixed samples that displayed a clear striation pattern
652 and a clear M-line (therefore, we conclude the muscles were in a stretched configuration). Zasp
653 was used as a marker for Z-discs, we traced a line spanning three contiguous Z-discs. The line
654 intensity plot of Phalloidin was obtained and was normalized by calculating deviation from the
655 mean to account for background noise; those with values above zero were used to calculate thin
656 filament length.
657
658 **Intensity quantification at the muscle ends (MTJs)**
659 Maximum intensity projections of confocal z-stacks of β_{PS}-Integrin, Talin and pTyr
660 immunostainings were generated in Fiji. A line spanning the MTJ and three contiguous
661 sarcomeres (as a landmark reference) was drawn with the line tool. Line intensity plots were
662 obtained with the intensity value for each pixel in the line. These values were split into five bins
663 (each bin encompassing 20% of the intensity values) along the anterior-posterior axis and an
664 average was calculated for each bin. Normalization was accomplished by calculating the deviation
665 from the mean value. We traced two lines per MTJ per larva (16-20 measurements per genotype
666 from 4-5 different larvae) and per genotype. This analysis was done in duplicate.
667

668 **Nuclear analysis**

669 All images were processed and analyzed with Fiji. 2D quantifications of VL3 and VL4 muscles
670 were performed with maximum intensity projections (as previously described in Windner et al.
671 (2019)). Muscle areas were traced by hand with the polygon tool. Automated thresholding of
672 fluorescence intensities of anti-Lamin and/or Hoechst was used to generate binary images of VL
673 nuclei. The number, size (area), position (X and Y coordinates) and shape descriptors (roundness
674 and circularity) of all nuclei within each cell was obtained and the binary masks were used to
675 quantify Hoechst and H3K9ac pixel intensity (mean gray value). Automated thresholding of anti-
676 Fibrillarin labeling was used to generate binary images of nucleoli and measure nucleolar sizes
677 (areas) and to quantify Fibrillarin pixel intensity (mean gray value). The 3D rendering of nuclei
678 was processed with Imaris.

679

680 **RNA sequencing analysis**

681 Eight to ten late third instar larvae were dissected as described above per genotype in each
682 replicate. The experiment was done in triplicate. The muscle-enriched larval filets were transferred
683 to TRIzol and homogenized. The lysates were submitted to the MSKCC's Integrated Genomics
684 Operations (IGO) core for further total RNA extraction, quality assessment and Illumina next-
685 generation sequencing. The sequencing libraries were constructed using SMARTerAmpSeq after
686 the mRNAs were enriched by oligo-dT-mediated purification. The libraries were then sequenced
687 on the Illumina HiSeq 4000 in a PE50 run. Over 40 million reads were generated per library.
688 FASTQ data was read into R with the ShortRead package (Morgan et al., 2009) and QC was
689 performed with the Rfastp package (Wang et al., 2022). Reads were mapped and aligned to the
690 *Drosophila* genome using Rsubread (Liao et al., 2019). Next, the reads were counted with the
691 GenomicAlignments package (Lawrence et al., 2013). Gene differential expression tests were
692 performed using DESeq2 (Love et al., 2014). Finally, enrichment analysis was performed through
693 goseq (Young et al., 2010) using both Gene Ontology and KEGG databases. Plots were drawn
694 using R with the ggplot2 package (Wickham, 2016).

695

696 **ATP assay**

697 An ATP calibration curve was performed using the stabilized ATP standard stocks provided in the
698 kit ATP Bioluminescence Assay Kit HS II (Millipore Sigma #11699709001) and following the
699 supplied protocol. Five to ten late third instar wandering larvae from each genotype were
700 dissected (See Immunolabeling and Imaging) and transferred into the cell lysis reagent provided
701 with the kit. Lysates were homogenized and protein concentrations were determined using the

Bradford assay. Equal amounts of protein (10 μg) were used for bioluminescence measurements. Blank measurements were subtracted from the raw data and ATP concentrations were calculated from the standard curve data. The experiment was done in triplicate.

Statistical analysis

Statistical significance was determined by either student's unpaired t-test (comparisons between two groups), one-way ANOVA, or two-way ANOVA (comparisons among multiple groups) in the GraphPad Prism software. Data are presented as mean±SD, asterisks are used to denote significance. Graphs were made using either GraphPad Prism, Microsoft Excel or R.

ACKNOWLEDGEMENTS

We thank the Baylies lab members, F. Schnorrer, G. Tanentzapf, A. Beggs and V. Gupta for helpful discussions and H. Bellen and F. Schöck for providing antibodies. We thank the members of the Integrated Genomics Operation (IGO) and the Bioinformatics Cores at MSKCC.

COMPETING INTERESTS

The authors declare no competing interests.

FUNDING

This work was supported by National Institutes of Health grant R01 GM073791 to R.D., a Blavatnik Family Foundation predoctoral fellowship to P.J.C., National Institutes of Health grants R01 AR068128 and R35 GM141877 to M.K.B., and the National Cancer Institute P30 CA 008748 to Memorial Sloan Kettering Cancer Center (MSKCC).

DATA AVAILABILITY

RNA-seq data have been deposited in Gene Expression Omnibus (GEO) under the accession number GSE210507.

732 **FIGURES**

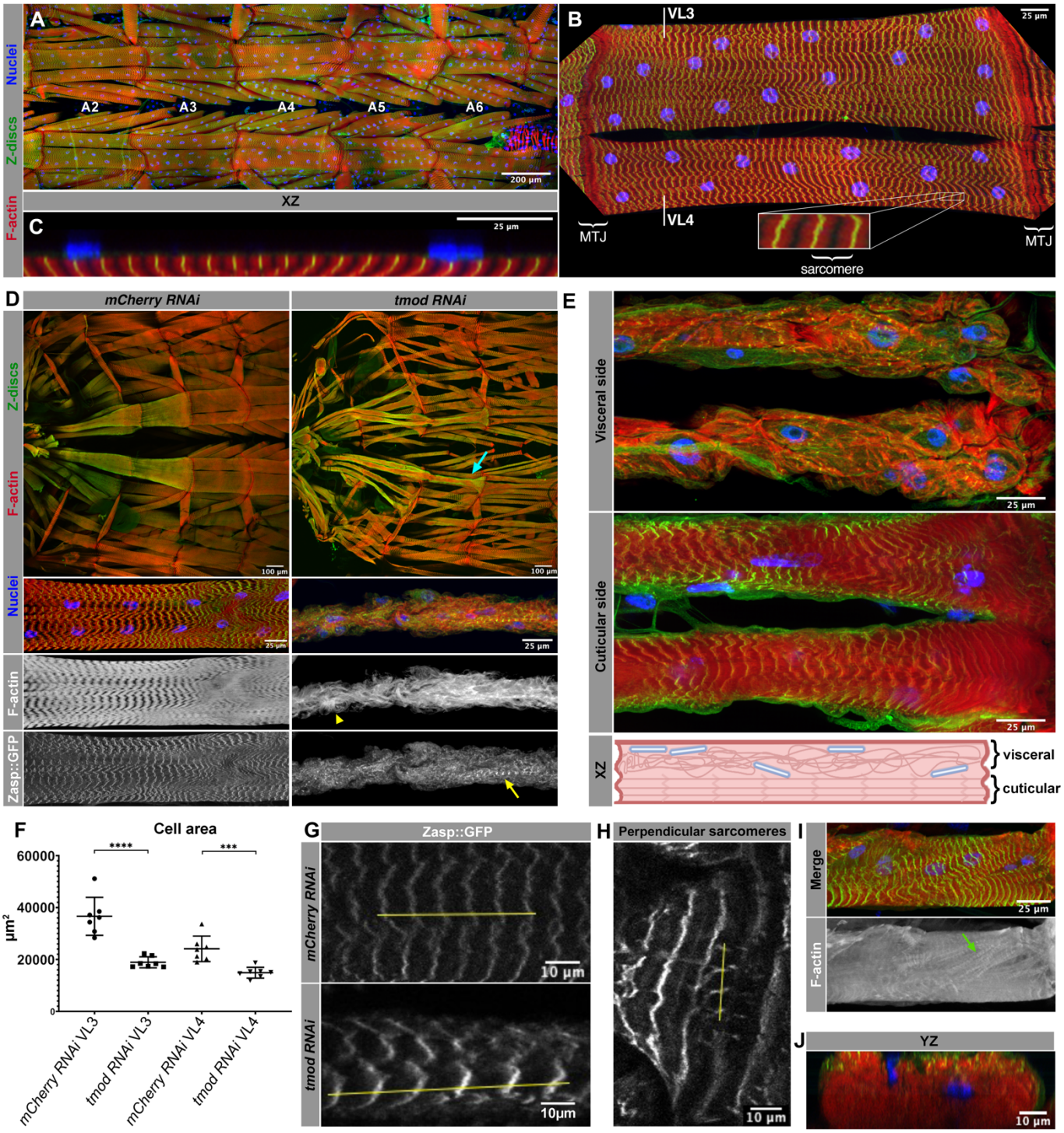

733

734 **Fig. 1: Tmod is required for larval muscle integrity.**

735 (A) Third instar *Drosophila* larval filet, abdominal segments (A2-6) and body wall muscles (red,

736 phalloidin) with Z-discs (green, Zasp::GFP) and nuclei (blue, Hoechst); anterior, left.

737 (B) VL3 and VL4 muscles showing MTJs and zoomed-in panel of a sarcomere (Z-stack
738 projection).
739 (C) VL4 myofiber longitudinal cross-section with nuclei on the cell surface.
740 (D) Overview of anterior musculature in control (*mCherryRNAi*) and Tmod-KD (*tmodRNAi*) larvae
741 (top). Higher magnification of VL3 muscle merge, F-actin and Zasp::GFP (bottom 3 panels). Cyan
742 arrow indicates width reduction of the myofiber. Yellow arrowhead: ectopic F-actin. Yellow arrow:
743 remaining myofibril.
744 (E) Visceral view of VL3 and VL4 Tmod-KD myofibers showing disorganized myofibrils and
745 ectopic F-actin (top), cuticular view showing conserved sarcomeres (middle) and cross-sectional
746 diagram showing integration of both visceral and cuticular sides in a myofiber (bottom).
747 (F) VL3 and VL4 myofiber areas (A2) in control and Tmod-KD wandering late third instars. Graph
748 represents one experiment (N>3 replicates, each with n_{VL3}=7 myofibers and n_{VL4}=7 myofibers per
749 genotype; p_{VL3}<0.0001 and p_{VL4}=0.0006, two-tailed unpaired Student's t-test). Mean ± SD.
750 (G) Sarcomere length in control and Tmod-KD myofibers. Yellow line spans six Z-discs.
751 (H) Perpendicular sarcomeres in Tmod-KD myofibers. Yellow line spans four Z-discs.
752 (I) Disorganized, misoriented myofibrils. Green arrow indicates diagonal myofibrils.
753 (J) Optical cross-section of Tmod-KD myofiber displaying internalized and misshapen nuclei.
754 Scale bars: 200μm (A), 100μm (top panels in D), 25μm (B, C, bottom 3 panels in D, E, and I) and
755 10μm (G, H, and J).

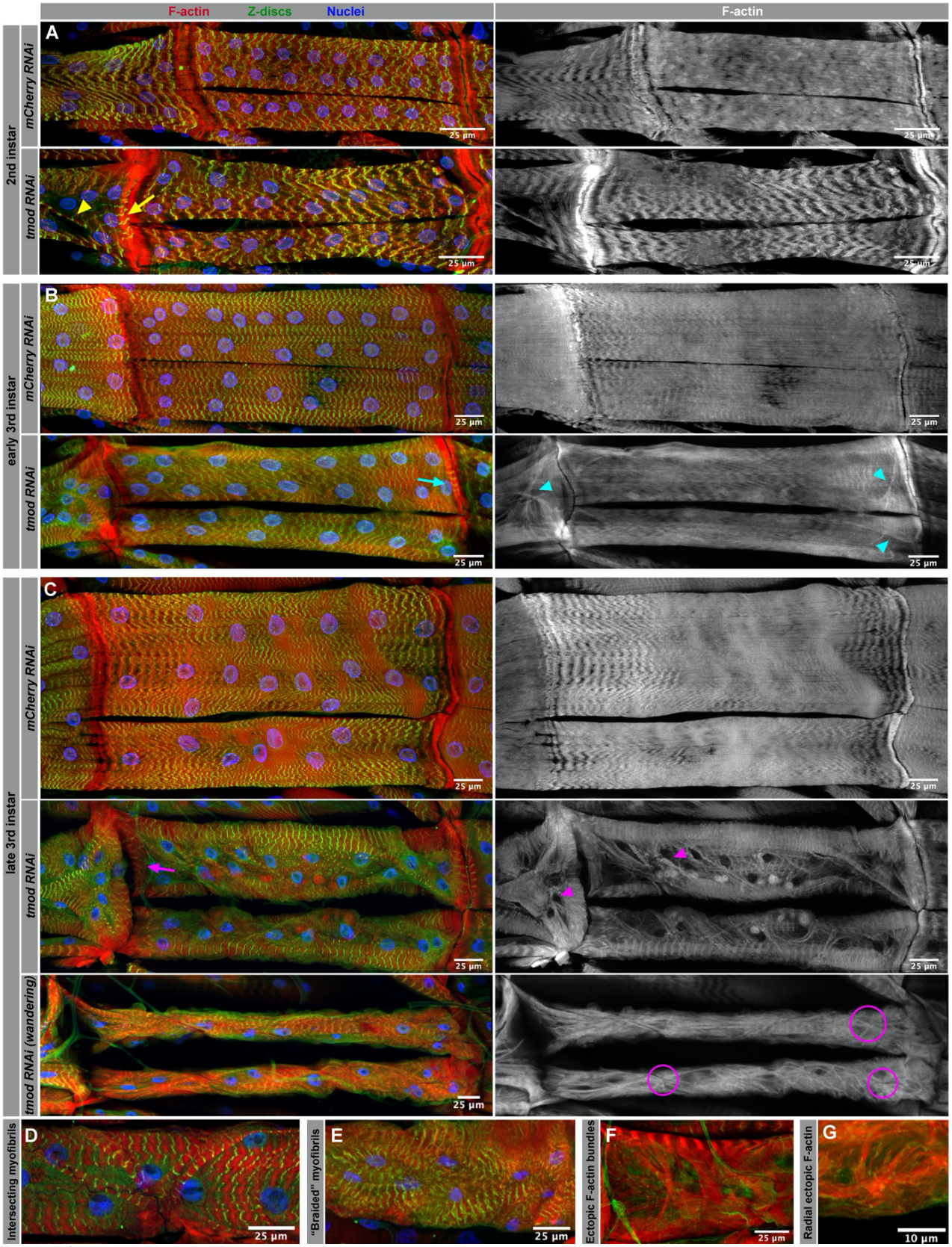
F-actin
Z-discs
Nuclei
F-actin
A
B
C
D
E
F
G
2nd instar
early 3rd instar
late 3rd instar
mCherry RNAi
tmod RNAi
tmod RNAi (wandering)
Intersecting myofibrils
"Braided" myofibrils
Ectopic F-actin bundles
Radial ectopic F-actin
25 µm
10 µm

Figure 2

757 **Fig. 2: Structural patterned deterioration of Tmod-KD myofibers throughout *Drosophila***
758 **larval stages.**
759 (A) Posterior end of VI1 myofiber from A1 segment and full length VL3 and VL4 myofibers from
760 A2 segment in control and Tmod-KD second instar larvae (red, phalloidin; green, Zasp::GFP and
761 blue, Hoechst) (left). F-actin channel only (gray, phalloidin) (right). Yellow arrowhead: diagonally
762 misoriented myofibril in VI1 from A1. Yellow arrow: perpendicular misoriented myofibrils in VI1
763 from A1.
764 (B) Worsening myofibers from A1 and A2 segment in Tmod-KD early third instars (bottom),
765 controls (top). Cyan arrowheads: diagonally misoriented myofibrils. Cyan arrow: perpendicular
766 myofibrils in posterior end of VL3 muscle from A2.
767 (C) Worsening myofibers from A1 and A2 in Tmod-KD late third instars (middle panels) and
768 wandering late third instar (bottom panel), control (top panel). Magenta arrowheads: worsening
769 of diagonally misoriented myofibrils from A1 and A2. Magenta arrow: perpendicular myofibrils in
770 anterior end of VL3 muscle from A2. Magenta circles: ectopic F-actin structures that replace
771 stereotypical myofibrillar pattern. Quantifications across the A-P axis in Supplemental Fig2D.
772 (D) Intersecting grouped myofibrils in early third instar.
773 (E) Interlaced or “braided” myofibrils in late third instar.
774 (F and G) Ectopic F-actin bundles and radial actin structures, respectively, that lack myofibrillar
775 pattern in wandering late third instar.
776 N=3 replicates, each with n=5 larvae per stage
777 Scale bars: 25μm (A-F) and 10μm (G).
778

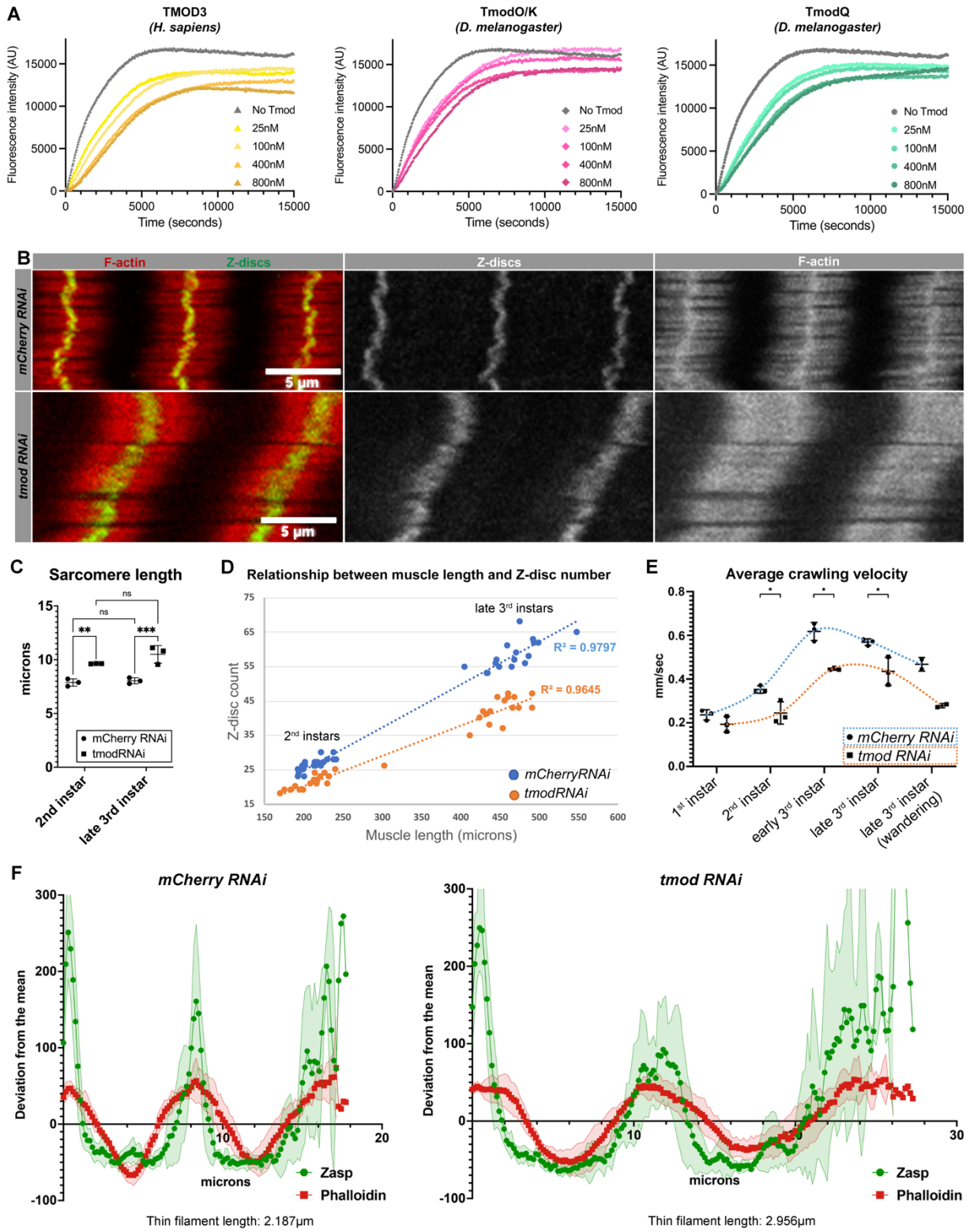

Fig. 3: *Drosophila* Tmod is a capping protein and Tmod-KD myofibers display longer thin filaments and sarcomeres.

782 (A) Pyrene-labeled actin polymerization assays at the pointed-end with human TMOD3,
783 *Drosophila* TmodO/K and TmodQ at multiple concentrations (N=4 per isoform per concentration).
784 (B) Cuticular sarcomeres from control and Tmod-KD myofibers of late third instars in A2 (red,
785 phalloidin, and green, Zasp) (left). Middle panel: Zasp channel; right panel: phalloidin channel.
786 (C) Sarcomere length in control and Tmod-KD VL3 myofibers from A2 in second instars and late
787 third instars. Each dot is one experiment (N=3 replicates, each with $n_{2nd\ instars}$=75-135, $n_{late\ 3rd}$
788 $_{instars}$=45-105 sarcomeres [from 3-8 different larvae] per genotype; $p_{2nd\ instars}$=0.0076, p_{3rd}
789 $_{instars}$=0.0009, $p_{mCherryRNAi}$=0.9703, $p_{tmodRNAi}$=0.1843, ordinary 2-way ANOVA multiple comparisons).
790 Mean ± SD.
791 (D) Scatterplots and regression lines (dotted) comparing Z-disc number in relationship to muscle
792 length (in microns) in control (blue) and Tmod-KD (orange) VL3 myofibers from A2 in second
793 instars and late third instars (N=3 experiments, each with $n_{2nd\ instars}$=19-20, $n_{late\ 3rd\ instars}$=16-17
794 myofibers per genotype). R^2 are indicated.
795 (E) Crawling velocities from each larval stage in control (blue) and Tmod-KD (orange). Each dot
796 is one experiment (N=3 replicates, $n_{1st\ instars}$=10, $n_{2nd\ instars}$=10, $n_{early\ 3rd\ instars}$=5-10, $n_{late\ 3rd\ instars}$= 3-
797 10, $n_{wandering}$=3-4 larvae per genotype and experiment; $p_{1st\ instars}$=0.245, $p_{2nd\ instars}$=0.0326, $p_{early\ 3rd}$
798 $_{instars}$=0.0182, $p_{late\ 3rd\ instars}$=0.0433, $p_{wandering}$=0.0507, two-tailed paired Student's t-test). Mean ± SD.
799 (F) Intensities of phalloidin (red) and Zasp::GFP (green) normalized as the deviation from the
800 mean and plotted across the length of two sarcomeres in A2 of late third instars. Thin filament
801 length is obtained from the length under the center peak divided in half (n=4-6 muscles from
802 different larva per genotype). Mean ± SD.
803 Scale bars: 5μm (B).
804

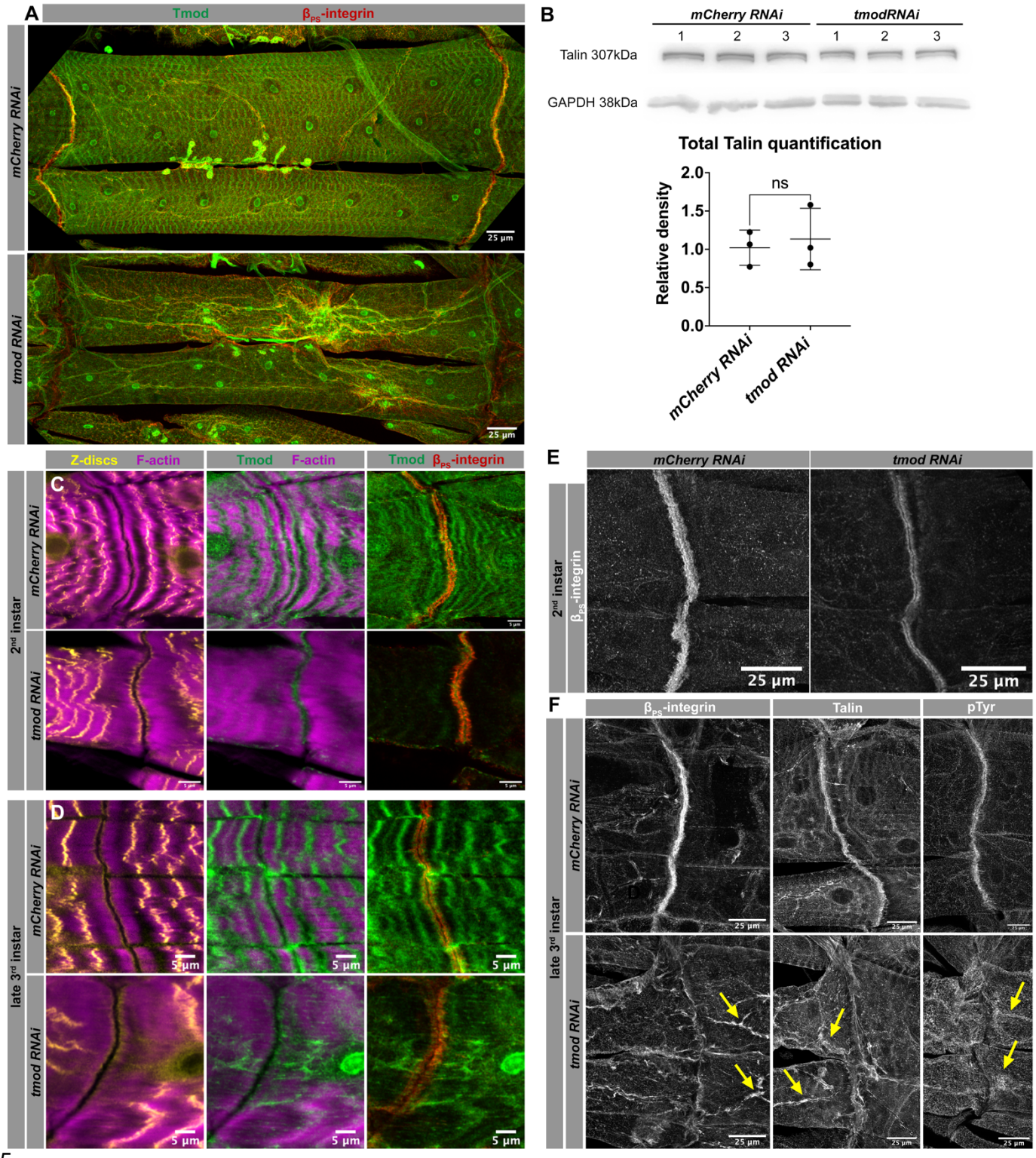

Fig. 4: Tmod-KD muscles exhibit Tmod decrease and loss of mechanosensory protein enrichment and tension at the MTJ.

(A) VL3 and VL4 myofibers in A2 from late third instars in control and Tmod-KD larvae. In control, Tmod (green) displays a stereotypical pattern in the sarcomeres and its colocalization with β_{PS}-

810 integrin (red) at the MTJ (top panel). In Tmod-KD myofibers, Tmod is not present at the same
811 intensity levels at the sarcomeres nor the MTJ (bottom panel).
812 (B) Talin Western blot and quantification in late third instar muscle-enriched lysates.
813 Glyceraldehyde 3-phosphate dehydrogenase (GAPDH), loading control. Each dot is an
814 experiment (N=3 replicates, each with n=5-10 larval carcasses per genotype, p=0.7846, two-
815 tailed paired Student's t-test). Mean ± SD.
816 (C and D) Analysis of protein localization (magenta, phalloidin; yellow, Zasp::GFP; green, Tmod;
817 and red, β_{PS}-integrin) relative to one another at the MTJ (A2-3) in control and Tmod-KD in second
818 and late third instar larvae.
819 (E) β_{PS}-integrin (white) strong enrichment at the MTJ (A2-3) in second instar control compared to
820 decreased signal in Tmod-KD. Quantification in Supplemental Fig 5A.
821 (F) β_{PS}-integrin (left), Talin (white, middle) and pTyr (white, right) strong enrichment at the MTJ
822 (A2-3) in wandering third instar control compared to absence of signal in Tmod-KD.
823 Quantifications in Supplemental Fig 5B. Yellow arrows: ectopic pools of protein.
824 Scale bars: 5μm (C, D) and 25μm (A, E, and F).
825

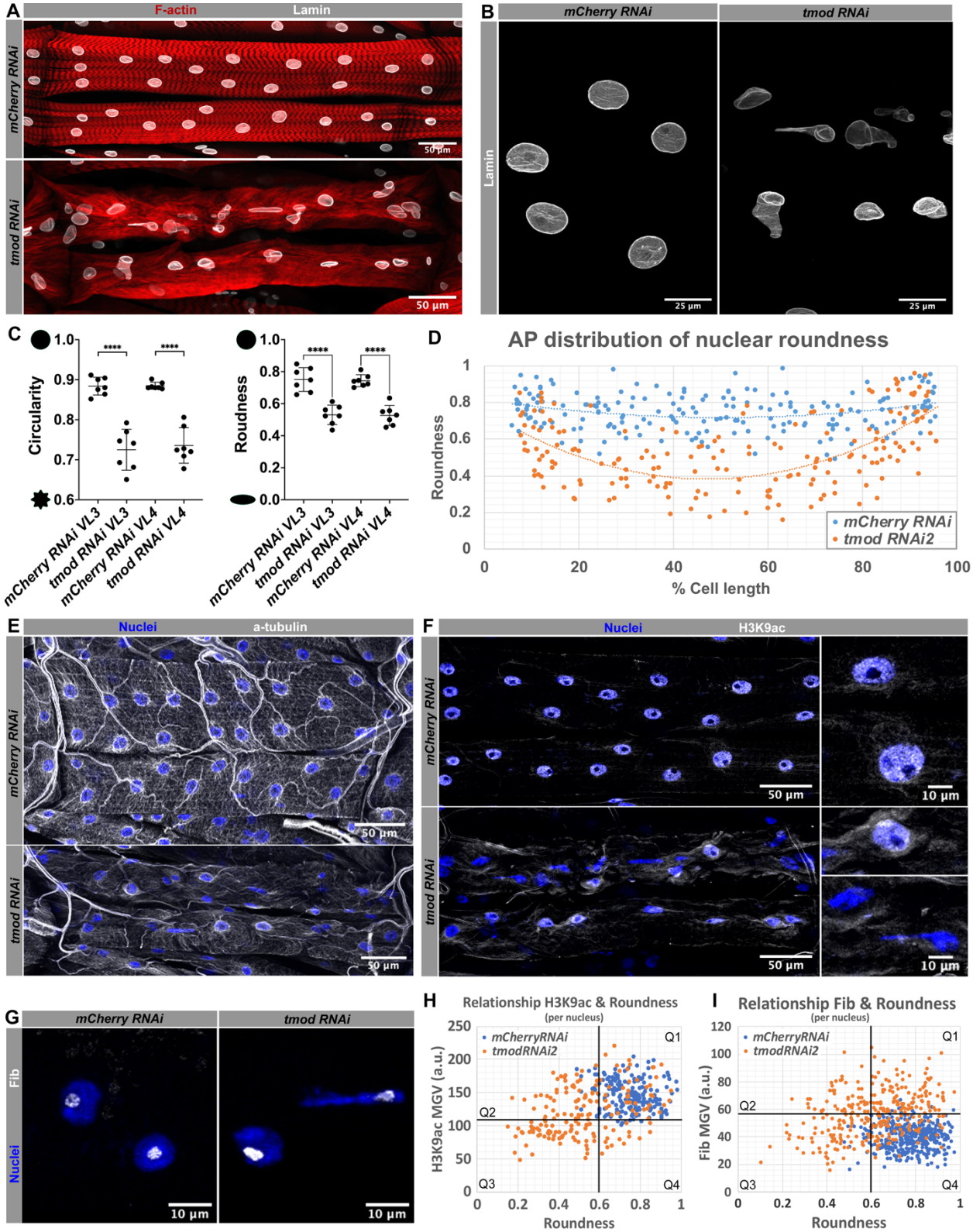

Fig. 5: Tmod-KD myofibers display misshapen and dysfunctional nuclei in late third instars.

829 (A) VL3 and VL4 myofibers (red, phalloidin) with nuclei (white, Lamin) in A2 in control (top) and
830 Tmod-KD larvae (bottom).
831 (B) High magnification of control myonuclei (white, Lamin) and misshapen and internalized Tmod-
832 KD nuclei. See supplemental Movie 1 and 2.
833 (C) Quantification of two shape descriptors: circularity and roundness in VL3 and VL4 myofibers
834 in A2 from control and Tmod-KD. Graph represents one experiment, each dot is one myofiber per
835 larva (n_{VL3}= 15-20, n_{VL4}=8-11 myonuclei per myofiber and genotype; circularity $p_{VL3}<0.0001$,
836 circularity $p_{VL4}<0.0001$; roundness $p_{VL3}<0.0001$, roundness $p_{VL4}<0.0001$, ordinary one-way
837 ANOVA multiple comparisons). Experiment repeated N>3. Mean±SD.
838 (D) Distribution of nuclear roundness along the AP axis of the myofiber from control (blue) and
839 Tmod-KD (orange) myofibers. Polynomial trendline shown by curved dotted lines.
840 (E) MT staining (white, α-tubulin; blue, nuclei) showing radial perinuclear arrays and longitudinal
841 tracks in control and a decrease of these in Tmod-KD.
842 (F-G) H3K9ac and Fib staining (white) indicating active transcription sites and nucleolus
843 respectively in myonuclei both in control and Tmod-KD myofibers.
844 (H and I) Scatterplots showing H3K9ac and Fib pixel intensity levels (mean gray value) in
845 relationship to roundness levels. Each graph represents one experiment, each dot is one
846 myonucleus (n_{H3K9ac}=178-190 myonuclei per genotype, from 7 VL3 and VL4 muscles sets, in 7
847 larvae; n_{Fib}=308-396 myonuclei per genotype, from 12-15 VL3 and VL4 muscle sets, in 7-8
848 larvae). (H) Q3 indicates Tmod-KD misshaped nuclei (roundness<0.6) with decreased H3K9ac
849 intensity when compared to control in Q1. (I) Q1 indicates Tmod-KD WT-like nuclei
850 (roundness>0.6) with increased Fib intensity when compared to control in Q4. Q3 indicate Tmod-
851 KD misshaped nuclei (roundness<0.6) with a similar Fib intensity when compared to control.
852 Experiments repeated N>2 unless specified otherwise.
853 Scale bars: 50μm (A, E and F), 25μm (B) and 10μm (F and G).
854

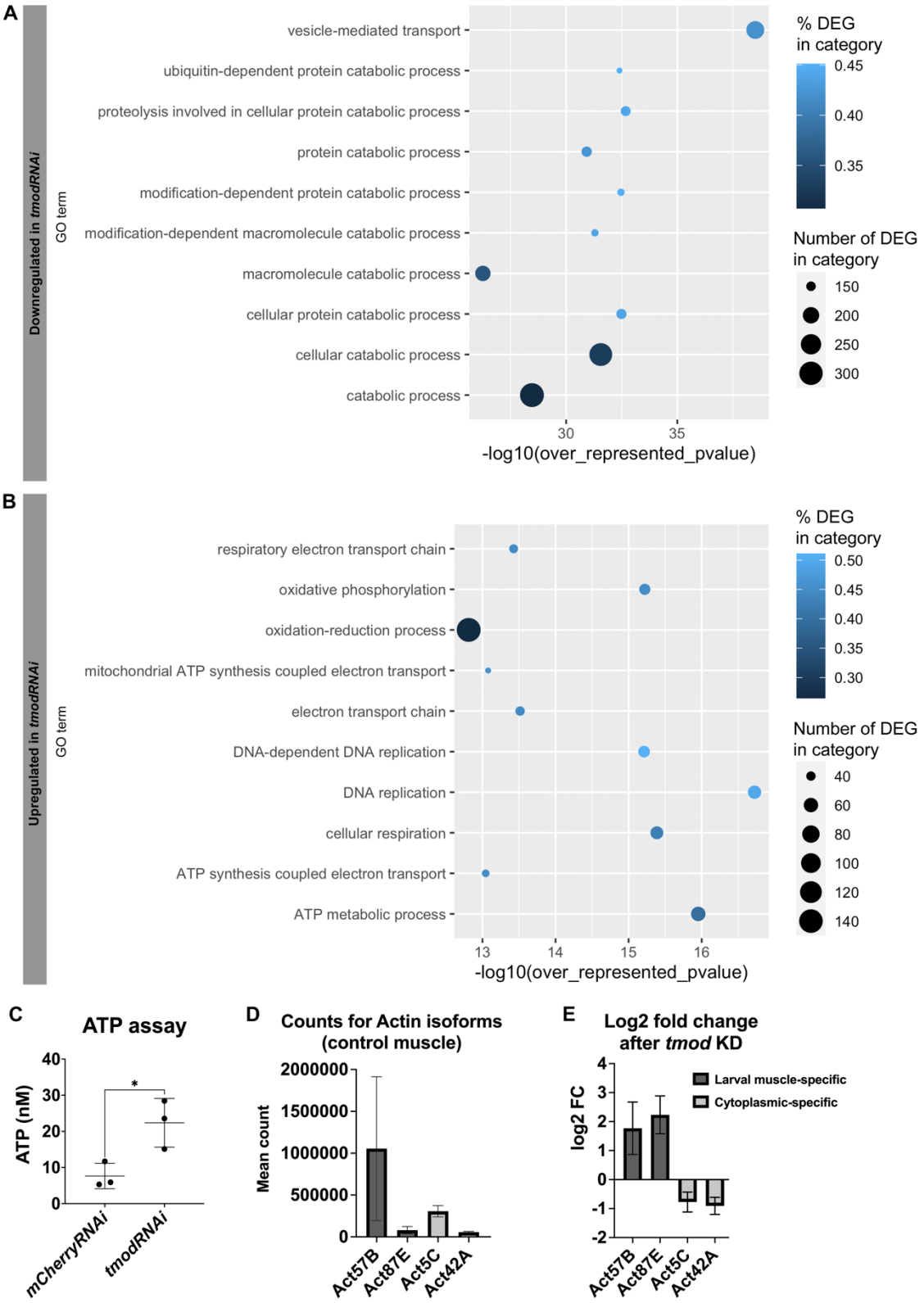

855

856 **Fig. 6: Tmod-KD late third instar larvae show differential gene expression (DEG).**

857 (A and B) Top 10 downregulated and upregulated Gene Ontology gene sets in Tmod-KD vs
858 control by ORA.
859 (C) ATP concentration in muscle-enriched larval lysates. Each dot is one experiment (N=3
860 replicates, each with n=5-10 larval carcasses per genotype, p=0.0285, two-tailed unpaired
861 Student's t-test). Mean ± SD.
862 (D) Normalized counts for the different *Drosophila* actin genes in control larvae. Mean ± SD.
863 (E) Log2 fold change of actin genes isoforms in Tmod-KD vs control (p_{Act57B}=0.0053,
864 p_{Act87E}<0.0001, p_{Act5E}= 0.0011, p_{Act42A}<0.0001). Mean±SE. RNAseq data was used for plots A, B,
865 D, and E (N=3 replicates, each with n=7-10 larval carcasses per genotype).
866

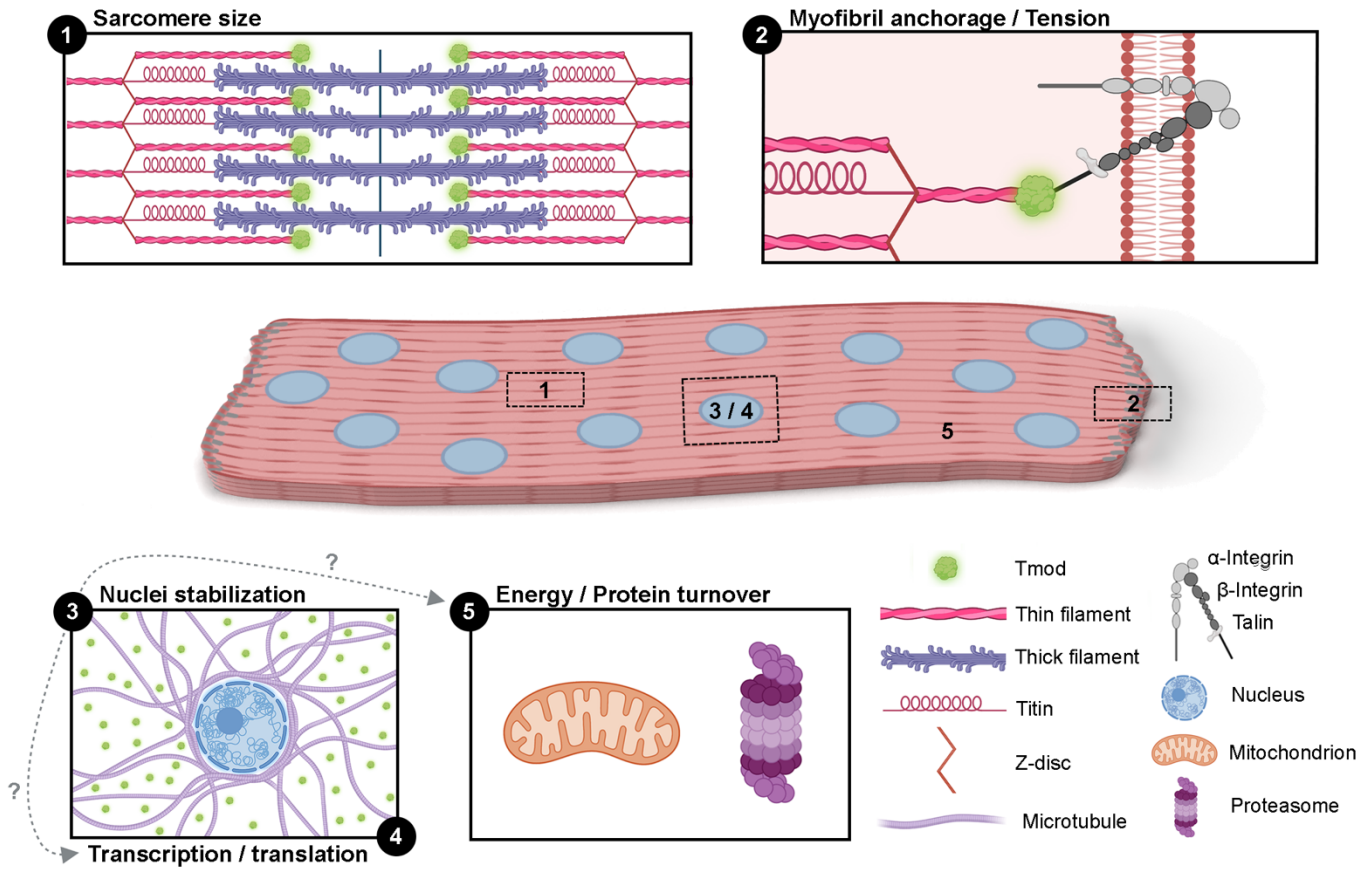

Fig. 7: Summary of Tmod's diverse roles in *Drosophila* larva myofibers.
(1) Sarcomere size: Tmod regulates sarcomere and thin filament length.
(2) Myofibril anchorage: Tmod establishes tension along the longitudinal axis by stabilizing the interaction of β_{PS}-integrin/Talin at the MTJ.
(3) Nuclear stabilization: Tmod maintains nuclear integrity either through MT-actin interactions or through nuclear F-actin.
(4) Transcription/translation: Tmod regulates nuclear output, through actin as a transcription factor in the nucleus or by actin's role in nuclear architecture and chromatin organization.
(5) Energy/Protein turnover: Upon Tmod-KD, we observed an increase in energy production genes and a decrease of proteasome genes. This change in transcriptome could be due to Tmod's role in nuclear stabilization or as compensation to generate myofiber growth.
Grey dashed arrows and question marks indicate potential consequences.

881 **REFERENCES**

882

883 ATHERTON, P., STUTCHBURY, B., JETHWA, D. & BALLESTREM, C. 2016.
884 Mechanosensitive components of integrin adhesions: Role of vinculin. *Exp Cell Res,* 343**,**
885 21-27.

886 AVELLANEDA, J., RODIER, C., DAIAN, F., BROUILLY, N., RIVAL, T., LUIS, N. M. &
887 SCHNORRER, F. 2021. Myofibril and mitochondria morphogenesis are coordinated by a
888 mechanical feedback mechanism in muscle. *Nat Commun,* 12**,** 2091.

889 BAI, J., HARTWIG, J. H. & PERRIMON, N. 2007. SALS, a WH2-domain-containing protein,
890 promotes sarcomeric actin filament elongation from pointed ends during Drosophila
891 muscle growth. *Dev Cell,* 13**,** 828-42.

892 BALAKRISHNAN, M., SISSO, W. J. & BAYLIES, M. K. 2021. Analyzing muscle structure and
893 function throughout the larval instars in live Drosophila. *STAR Protoc,* 2**,** 100291.

894 BALAKRISHNAN, M., YU, S. F., CHIN, S. M., SOFFAR, D. B., WINDNER, S. E., GOODE, B.
895 L. & BAYLIES, M. K. 2020. Cofilin Loss in Drosophila Muscles Contributes to Muscle
896 Weakness through Defective Sarcomerogenesis during Muscle Growth. *Cell Rep,* 32**,**
897 107893.

898 BAROHN, R. J., DIMACHKIE, M. M. & JACKSON, C. E. 2014. A pattern recognition approach
899 to patients with a suspected myopathy. *Neurol Clin,* 32**,** 569-93, vii.

900 BATE, M. 1990. The embryonic development of larval muscles in Drosophila. *Development,*
901 110**,** 791-804.

902 BAWA, S., BROOKS, D. S., NEVILLE, K. E., TIPPING, M., SAGAR, M. A., KOLLHOFF, J. A.,
903 CHAWLA, G., GEISBRECHT, B. V., TENNESSEN, J. M., ELICEIRI, K. W. &
904 GEISBRECHT, E. R. 2020. Drosophila TRIM32 cooperates with glycolytic enzymes to
905 promote cell growth. *Elife,* 9.

906 BECKER, R., LEONE, M. & ENGEL, F. B. 2020. Microtubule Organization in Striated Muscle
907 Cells. *Cells,* 9.

908 BERGER, J., BERGER, S., MOK, Y. S. G., LI, M., TARAKCI, H. & CURRIE, P. D. 2022.
909 Genetic dissection of novel myopathy models reveals a role of CapZalpha and Leiomodin
910 3 during myofibril elongation. *PLoS Genet,* 18**,** e1010066.

911 BERGER, J., TARAKCI, H., BERGER, S., LI, M., HALL, T. E., ARNER, A. & CURRIE, P. D.
912 2014. Loss of Tropomodulin4 in the zebrafish mutant trage causes cytoplasmic rod
913 formation and muscle weakness reminiscent of nemaline myopathy. *Dis Model Mech,* 7**,**
914 1407-15.

915 BETTINGER, B. T., GILBERT, D. M. & AMBERG, D. C. 2004. Actin up in the nucleus. *Nat Rev*
916 *Mol Cell Biol,* 5**,** 410-5.
917 BODENSTEIN, D. 1950. The Postembryonic Development of Drosophila. *In:* M, D. (ed.)
918 *Biology of Drosophila.* Cold Spring Harbor Laboratory Press.
919 BRAND, A. H. & PERRIMON, N. 1993. Targeted gene expression as a means of altering cell
920 fates and generating dominant phenotypes. *Development,* 118**,** 401-15.
921 BRENT, J. R., WERNER, K. M. & MCCABE, B. D. 2009. Drosophila larval NMJ dissection. *J*
922 *Vis Exp*.
923 BROOKS, D., BAWA, S., BONTRAGER, A., STETSIV, M., GUO, Y. & GEISBRECHT, E. R.
924 2022. Independent pathways control muscle tissue size and sarcomere remodeling. *Dev*
925 *Biol,* 490**,** 1-12.
926 CARIDI, C. P., PLESSNER, M., GROSSE, R. & CHIOLO, I. 2019. Nuclear actin filaments in
927 DNA repair dynamics. *Nat Cell Biol,* 21**,** 1068-1077.
928 CENIK, B. K., GARG, A., MCANALLY, J. R., SHELTON, J. M., RICHARDSON, J. A., BASSEL-
929 DUBY, R., OLSON, E. N. & LIU, N. 2015. Severe myopathy in mice lacking the
930 MEF2/SRF-dependent gene leiomodin-3. *J Clin Invest,* 125**,** 1569-78.
931 CHANG, W., ANTOKU, S., OSTLUND, C., WORMAN, H. J. & GUNDERSEN, G. G. 2015.
932 Linker of nucleoskeleton and cytoskeleton (LINC) complex-mediated actin-dependent
933 nuclear positioning orients centrosomes in migrating myoblasts. *Nucleus,* 6**,** 77-88.
934 CHARVET, B., RUGGIERO, F. & LE GUELLEC, D. 2012. The development of the
935 myotendinous junction. A review. *Muscles Ligaments Tendons J,* 2**,** 53-63.
936 CHASE, P. B., SZCZYPINSKI, M. P. & SOTO, E. P. 2013. Nuclear tropomyosin and troponin
937 in striated muscle: new roles in a new locale? *J Muscle Res Cell Motil,* 34**,** 275-84.
938 CHEREAU, D., BOCZKOWSKA, M., SKWAREK-MARUSZEWSKA, A., FUJIWARA, I.,
939 HAYES, D. B., REBOWSKI, G., LAPPALAINEN, P., POLLARD, T. D. & DOMINGUEZ, R.
940 2008. Leiomodin is an actin filament nucleator in muscle cells. *Science,* 320**,** 239-43.
941 CHRISTOPHERS, B., LOPEZ, M. A., GUPTA, V. A., VOGEL, H. & BAYLIES, M. 2022.
942 Pediatric Nemaline Myopathy: A Systematic Review Using Individual Patient Data. *Journal*
943 *of Child Neurology,* 37**,** 652-663.
944 CHRZANOWSKA-WODNICKA, M. & BURRIDGE, K. 1994. Tyrosine phosphorylation is
945 involved in reorganization of the actin cytoskeleton in response to serum or LPA
946 stimulation. *J Cell Sci,* 107 (Pt 12)**,** 3643-54.
947 DAVIDSON, P. M. & CADOT, B. 2021. Actin on and around the Nucleus. *Trends Cell Biol,* 31**,**
948 211-223.

949 DE WINTER, J. M. & OTTENHEIJM, C. A. C. 2017. Sarcomere Dysfunction in Nemaline
950 Myopathy. *J Neuromuscul Dis,* 4**,** 99-113.
951 DEMONTIS, F. & PERRIMON, N. 2009. Integration of Insulin receptor/Foxo signaling and
952 dMyc activity during muscle growth regulates body size in Drosophila. *Development,* 136**,**
953 983-93.
954 DENG, S., SILIMON, R. L., BALAKRISHNAN, M., BOTHE, I., JUROS, D., SOFFAR, D. B. &
955 BAYLIES, M. K. 2021. The actin polymerization factor Diaphanous and the actin severing
956 protein Flightless I collaborate to regulate sarcomere size. *Dev Biol,* 469**,** 12-25.
957 DIX, D. J. & EISENBERG, B. R. 1990. Myosin mRNA accumulation and myofibrillogenesis at
958 the myotendinous junction of stretched muscle fibers. *J Cell Biol,* 111**,** 1885-94.
959 DLUGOSZ, A. A., ANTIN, P. B., NACHMIAS, V. T. & HOLTZER, H. 1984. The relationship
960 between stress fiber-like structures and nascent myofibrils in cultured cardiac myocytes.
961 *J Cell Biol,* 99**,** 2268-78.
962 DOGTEROM, M. & KOENDERINK, G. H. 2019. Actin-microtubule crosstalk in cell biology. *Nat*
963 *Rev Mol Cell Biol,* 20**,** 38-54.
964 DOOLITTLE, L. K., ROSEN, M. K. & PADRICK, S. B. 2013. Measurement and analysis of in
965 vitro actin polymerization. *Methods Mol Biol,* 1046**,** 273-93.
966 DYE, C. A., LEE, J. K., ATKINSON, R. C., BREWSTER, R., HAN, P. L. & BELLEN, H. J. 1998.
967 The Drosophila sanpodo gene controls sibling cell fate and encodes a tropomodulin
968 homolog, an actin/tropomyosin-associated protein. *Development,* 125**,** 1845-56.
969 FARINA, F., GAILLARD, J., GUERIN, C., COUTE, Y., SILLIBOURNE, J., BLANCHOIN, L. &
970 THERY, M. 2016. The centrosome is an actin-organizing centre. *Nat Cell Biol,* 18**,** 65-75.
971 FENG, Y., UEDA, A. & WU, C. F. 2004. A modified minimal hemolymph-like solution, HL3.1,
972 for physiological recordings at the neuromuscular junctions of normal and mutant
973 Drosophila larvae. *J Neurogenet,* 18**,** 377-402.
974 FENIX, A. M., NEININGER, A. C., TANEJA, N., HYDE, K., VISETSOUK, M. R., GARDE, R.
975 J., LIU, B., NIXON, B. R., MANALO, A. E., BECKER, J. R., CRAWLEY, S. W., BADER,
976 D. M., TYSKA, M. J., LIU, Q., GUTZMAN, J. H. & BURNETTE, D. T. 2018. Muscle-specific
977 stress fibers give rise to sarcomeres in cardiomyocytes. *Elife,* 7.
978 FERNANDES, I. & SCHOCK, F. 2014. The nebulin repeat protein Lasp regulates I-band
979 architecture and filament spacing in myofibrils. *J Cell Biol,* 206**,** 559-72.
980 FISCHER, R. S., YARMOLA, E. G., WEBER, K. L., SPEICHER, K. D., SPEICHER, D. W.,
981 BUBB, M. R. & FOWLER, V. M. 2006. Tropomodulin 3 binds to actin monomers. *J Biol*
982 *Chem,* 281**,** 36454-65.

983 FOWLER, V. M. 1997. Capping actin filament growth: tropomodulin in muscle and nonmuscle
984 cells. *Soc Gen Physiol Ser,* 52**,** 79-89.
985 FOWLER, V. M. & DOMINGUEZ, R. 2017. Tropomodulins and Leiomodins: Actin Pointed End
986 Caps and Nucleators in Muscles. *Biophys J,* 112**,** 1742-1760.
987 FYRBERG, E. A., MAHAFFEY, J. W., BOND, B. J. & DAVIDSON, N. 1983. Transcripts of the
988 six Drosophila actin genes accumulate in a stage- and tissue-specific manner. *Cell,* 33**,**
989 115-23.
990 GHOSH, A. & FOWLER, V. M. 2021. Tropomodulins. *Curr Biol,* 31**,** R501-R503.
991 GILLERY, P., GEORGES, N., RANDOUX, A., LEFEVRE, F., MAQUART, F. X. & BOREL, J.
992 P. 1996. Modulation of protein synthesis by extracellular matrix: potential involvement of
993 two nucleolar proteins, nucleolin and fibrillarin. *Biochem Biophys Res Commun,* 228**,** 94-
994 9.
995 GOKHIN, D. S. & FOWLER, V. M. 2013. A two-segment model for thin filament architecture in
996 skeletal muscle. *Nat Rev Mol Cell Biol,* 14**,** 113-9.
997 GOLDSPINK, G. 1983. Alterations in Myofibril Size and Structure During Growth, Exercise,
998 and Changes in Environmental Temperature. *Comprehensive Physiology.*
999 GREGORIO, C. C., WEBER, A., BONDAD, M., PENNISE, C. R. & FOWLER, V. M. 1995.
1000 Requirement of pointed-end capping by tropomodulin to maintain actin filament length in
1001 embryonic chick cardiac myocytes. *Nature,* 377**,** 83-6.
1002 HAAS, J. N. 1950. Cytoplasmic growth in the muscle fibers of larvae of Drosophila
1003 melanogaster. *Growth,* 14**,** 277-94.
1004 KEE, A. J., GUNNING, P. W. & HARDEMAN, E. C. 2009. Diverse roles of the actin
1005 cytoskeleton in striated muscle. *J Muscle Res Cell Motil,* 30**,** 187-97.
1006 KHARCHENKO, P. V., ALEKSEYENKO, A. A., SCHWARTZ, Y. B., MINODA, A., RIDDLE, N.
1007 C., ERNST, J., SABO, P. J., LARSCHAN, E., GORCHAKOV, A. A., GU, T., LINDER-
1008 BASSO, D., PLACHETKA, A., SHANOWER, G., TOLSTORUKOV, M. Y., LUQUETTE, L.
1009 J., XI, R., JUNG, Y. L., PARK, R. W., BISHOP, E. P., CANFIELD, T. K., SANDSTROM,
1010 R., THURMAN, R. E., MACALPINE, D. M., STAMATOYANNOPOULOS, J. A., KELLIS,
1011 M., ELGIN, S. C., KURODA, M. I., PIRROTTA, V., KARPEN, G. H. & PARK, P. J. 2011.
1012 Comprehensive analysis of the chromatin landscape in Drosophila melanogaster. *Nature,*
1013 471**,** 480-5.
1014 KUMARI, R., JIU, Y., CARMAN, P. J., TOJKANDER, S., KOGAN, K., VARJOSALO, M.,
1015 GUNNING, P. W., DOMINGUEZ, R. & LAPPALAINEN, P. 2020. Tropomodulins Control

1016 the Balance between Protrusive and Contractile Structures by Stabilizing Actin-
1017 Tropomyosin Filaments. *Curr Biol,* 30**,** 767-778 e5.
1018 LABEAU-DIMENNA, E. M., CLARK, K. A., BAUMAN, K. D., PARKER, D. S., CRIPPS, R. M.
1019 & GEISBRECHT, E. R. 2012. Thin, a Trim32 ortholog, is essential for myofibril stability
1020 and is required for the integrity of the costamere in Drosophila. *Proc Natl Acad Sci U S A,*
1021 109**,** 17983-8.
1022 LAHIRI, S., SHEN, K., KLEIN, M., TANG, A., KANE, E., GERSHOW, M., GARRITY, P. &
1023 SAMUEL, A. D. 2011. Two alternating motor programs drive navigation in Drosophila
1024 larva. *PLoS One,* 6**,** e23180.
1025 LAITILA, J. & WALLGREN-PETTERSSON, C. 2021. Recent advances in nemaline myopathy.
1026 *Neuromuscul Disord,* 31**,** 955-967.
1027 LAWRENCE, M., HUBER, W., PAGES, H., ABOYOUN, P., CARLSON, M., GENTLEMAN, R.,
1028 MORGAN, M. T. & CAREY, V. J. 2013. Software for computing and annotating genomic
1029 ranges. *PLoS Comput Biol,* 9**,** e1003118.
1030 LEE, H. S., LIM, C. J., PUZON-MCLAUGHLIN, W., SHATTIL, S. J. & GINSBERG, M. H. 2009.
1031 RIAM activates integrins by linking talin to ras GTPase membrane-targeting sequences. *J*
1032 *Biol Chem,* 284**,** 5119-27.
1033 LEFEVRE, F., GARNOTEL, R., GEORGES, N. & GILLERY, P. 2001. Modulation of collagen
1034 metabolism by the nucleolar protein fibrillarin. *Exp Cell Res,* 271**,** 84-93.
1035 LEGOFF, L. & LECUIT, T. 2015. Mechanical Forces and Growth in Animal Tissues. *Cold*
1036 *Spring Harb Perspect Biol,* 8**,** a019232.
1037 LEMKE, S. B. & SCHNORRER, F. 2017. Mechanical forces during muscle development. *Mech*
1038 *Dev,* 144**,** 92-101.
1039 LEMKE, S. B., WEIDEMANN, T., COST, A. L., GRASHOFF, C. & SCHNORRER, F. 2019. A
1040 small proportion of Talin molecules transmit forces at developing muscle attachments in
1041 vivo. *PLoS Biol,* 17**,** e3000057.
1042 LIAO, Y., SMYTH, G. K. & SHI, W. 2019. The R package Rsubread is easier, faster, cheaper
1043 and better for alignment and quantification of RNA sequencing reads. *Nucleic Acids Res,*
1044 47**,** e47.
1045 LITTLEFIELD, R., ALMENAR-QUERALT, A. & FOWLER, V. M. 2001. Actin dynamics at
1046 pointed ends regulates thin filament length in striated muscle. *Nat Cell Biol,* 3**,** 544-51.
1047 LITTLEFIELD, R. S. & FOWLER, V. M. 2008. Thin filament length regulation in striated muscle
1048 sarcomeres: pointed-end dynamics go beyond a nebulin ruler. *Semin Cell Dev Biol,* 19**,**
1049 511-9.

1050 LIVAK, K. J. & SCHMITTGEN, T. D. 2001. Analysis of relative gene expression data using
1051 real-time quantitative PCR and the 2(-Delta Delta C(T)) Method. *Methods,* 25**,** 402-8.
1052 LOVE, M. I., HUBER, W. & ANDERS, S. 2014. Moderated estimation of fold change and
1053 dispersion for RNA-seq data with DESeq2. *Genome Biol,* 15**,** 550.
1054 MANHART, A., WINDNER, S., BAYLIES, M. & MOGILNER, A. 2018. Mechanical positioning
1055 of multiple nuclei in muscle cells. *PLoS Comput Biol,* 14**,** e1006208.
1056 MARDAHL-DUMESNIL, M. & FOWLER, V. M. 2001. Thin filaments elongate from their pointed
1057 ends during myofibril assembly in Drosophila indirect flight muscle. *J Cell Biol,* 155**,** 1043-
1058 53.
1059 MARTINO, F., PERESTRELO, A. R., VINARSKY, V., PAGLIARI, S. & FORTE, G. 2018.
1060 Cellular Mechanotransduction: From Tension to Function. *Front Physiol,* 9**,** 824.
1061 METZGER, T., GACHE, V., XU, M., CADOT, B., FOLKER, E. S., RICHARDSON, B. E.,
1062 GOMES, E. R. & BAYLIES, M. K. 2012. MAP and kinesin-dependent nuclear positioning
1063 is required for skeletal muscle function. *Nature,* 484**,** 120-4.
1064 MOHAMMAD, I., ARORA, P. D., NAGHIBZADEH, Y., WANG, Y., LI, J., MASCARENHAS, W.,
1065 JANMEY, P. A., DAWSON, J. F. & MCCULLOCH, C. A. 2012. Flightless I is a focal
1066 adhesion-associated actin-capping protein that regulates cell migration. *FASEB J,* 26**,**
1067 3260-72.
1068 MOLNAR, I., MIGH, E., SZIKORA, S., KALMAR, T., VEGH, A. G., DEAK, F., BARKO, S.,
1069 BUGYI, B., ORFANOS, Z., KOVACS, J., JUHASZ, G., VARO, G., NYITRAI, M.,
1070 SPARROW, J. & MIHALY, J. 2014. DAAM is required for thin filament formation and
1071 Sarcomerogenesis during muscle development in Drosophila. *PLoS Genet,* 10**,**
1072 e1004166.
1073 MORGAN, M., ANDERS, S., LAWRENCE, M., ABOYOUN, P., PAGES, H. & GENTLEMAN,
1074 R. 2009. ShortRead: a bioconductor package for input, quality assessment and
1075 exploration of high-throughput sequence data. *Bioinformatics,* 25**,** 2607-8.
1076 ONO, S. 2010. Dynamic regulation of sarcomeric actin filaments in striated muscle.
1077 *Cytoskeleton (Hoboken),* 67**,** 677-92.
1078 OTTENHEIJM, C. A., WITT, C. C., STIENEN, G. J., LABEIT, S., BEGGS, A. H. & GRANZIER,
1079 H. 2009. Thin filament length dysregulation contributes to muscle weakness in nemaline
1080 myopathy patients with nebulin deficiency. *Hum Mol Genet,* 18**,** 2359-69.
1081 PARDEE, J. D., SIMPSON, P. A., STRYER, L. & SPUDICH, J. A. 1982. Actin filaments
1082 undergo limited subunit exchange in physiological salt conditions. *J Cell Biol,* 94**,** 316-24.

1083 PARDO, J. V., SILICIANO, J. D. & CRAIG, S. W. 1983. A vinculin-containing cortical lattice in
1084 skeletal muscle: transverse lattice elements ("costameres") mark sites of attachment
1085 between myofibrils and sarcolemma. *Proc Natl Acad Sci U S A,* 80**,** 1008-12.
1086 PARSONS, J. T., HORWITZ, A. R. & SCHWARTZ, M. A. 2010. Cell adhesion: integrating
1087 cytoskeletal dynamics and cellular tension. *Nat Rev Mol Cell Biol,* 11**,** 633-43.
1088 PERKINS, L. A., HOLDERBAUM, L., TAO, R., HU, Y., SOPKO, R., MCCALL, K., YANG-
1089 ZHOU, D., FLOCKHART, I., BINARI, R., SHIM, H. S., MILLER, A., HOUSDEN, A., FOOS,
1090 M., RANDKELV, S., KELLEY, C., NAMGYAL, P., VILLALTA, C., LIU, L. P., JIANG, X.,
1091 HUAN-HUAN, Q., WANG, X., FUJIYAMA, A., TOYODA, A., AYERS, K., BLUM, A.,
1092 CZECH, B., NEUMULLER, R., YAN, D., CAVALLARO, A., HIBBARD, K., HALL, D.,
1093 COOLEY, L., HANNON, G. J., LEHMANN, R., PARKS, A., MOHR, S. E., UEDA, R.,
1094 KONDO, S., NI, J. Q. & PERRIMON, N. 2015. The Transgenic RNAi Project at Harvard
1095 Medical School: Resources and Validation. *Genetics,* 201**,** 843-52.
1096 PINES, M., DAS, R., ELLIS, S. J., MORIN, A., CZERNIECKI, S., YUAN, L., KLOSE, M.,
1097 COOMBS, D. & TANENTZAPF, G. 2012. Mechanical force regulates integrin turnover in
1098 Drosophila in vivo. *Nat Cell Biol,* 14**,** 935-43.
1099 QUACH, N. L. & RANDO, T. A. 2006. Focal adhesion kinase is essential for costamerogenesis
1100 in cultured skeletal muscle cells. *Dev Biol,* 293**,** 38-52.
1101 RAO, J. N., MADASU, Y. & DOMINGUEZ, R. 2014. Mechanism of actin filament pointed-end
1102 capping by tropomodulin. *Science,* 345**,** 463-7.
1103 ROMERO, N. B. 2010. Centronuclear myopathies: a widening concept. *Neuromuscul Disord,*
1104 20**,** 223-8.
1105 ROPER, K., MAO, Y. & BROWN, N. H. 2005. Contribution of sequence variation in Drosophila
1106 actins to their incorporation into actin-based structures in vivo. *J Cell Sci,* 118**,** 3937-48.
1107 ROSS, J. A., LEVY, Y., RIPOLONE, M., KOLB, J. S., TURMAINE, M., HOLT, M., LINDQVIST,
1108 J., CLAEYS, K. G., WEIS, J., MONFORTE, M., TASCA, G., MOGGIO, M., FIGEAC, N.,
1109 ZAMMIT, P. S., JUNGBLUTH, H., FIORILLO, C., VISSING, J., WITTING, N., GRANZIER,
1110 H., ZANOTELI, E., HARDEMAN, E. C., WALLGREN-PETTERSSON, C. & OCHALA, J.
1111 2019. Impairments in contractility and cytoskeletal organisation cause nuclear defects in
1112 nemaline myopathy. *Acta Neuropathol,* 138**,** 477-495.
1113 SANGER, J. M. & SANGER, J. W. 2008. The dynamic Z bands of striated muscle cells. *Sci*
1114 *Signal,* 1**,** pe37.
1115 SCHIAFFINO, S., DYAR, K. A., CICILIOT, S., BLAAUW, B. & SANDRI, M. 2013. Mechanisms
1116 regulating skeletal muscle growth and atrophy. *FEBS J,* 280**,** 4294-314.

1117 SCHMITTGEN, T. D. & LIVAK, K. J. 2008. Analyzing real-time PCR data by the comparative
1118 C(T) method. *Nat Protoc,* 3**,** 1101-8.
1119 SCHNORRER, F., SCHONBAUER, C., LANGER, C. C., DIETZL, G., NOVATCHKOVA, M.,
1120 SCHERNHUBER, K., FELLNER, M., AZARYAN, A., RADOLF, M., STARK, A.,
1121 KELEMAN, K. & DICKSON, B. J. 2010. Systematic genetic analysis of muscle
1122 morphogenesis and function in Drosophila. *Nature,* 464**,** 287-91.
1123 SEWRY, C. A., LAITILA, J. M. & WALLGREN-PETTERSSON, C. 2019. Nemaline myopathies:
1124 a current view. *J Muscle Res Cell Motil*.
1125 SHATTIL, S. J., KIM, C. & GINSBERG, M. H. 2010. The final steps of integrin activation: the
1126 end game. *Nat Rev Mol Cell Biol,* 11**,** 288-300.
1127 SHIRINIAN, M., POPOVIC, M., GRABBE, C., VARSHNEY, G., HUGOSSON, F., BOS, H.,
1128 REHMANN, H. & PALMER, R. H. 2010. The Rap1 guanine nucleotide exchange factor
1129 C3G is required for preservation of larval muscle integrity in Drosophila melanogaster.
1130 *PLoS One,* 5**,** e9403.
1131 SMILLIE, L. B. 1982. Preparation and identification of alpha- and beta-tropomyosins. *Methods*
1132 *Enzymol,* 85 Pt B**,** 234-41.
1133 SPARROW, J. C. & SCHOCK, F. 2009. The initial steps of myofibril assembly: integrins pave
1134 the way. *Nat Rev Mol Cell Biol,* 10**,** 293-8.
1135 SPLETTER, M. L., BARZ, C., YEROSLAVIZ, A., SCHONBAUER, C., FERREIRA, I. R.,
1136 SAROV, M., GERLACH, D., STARK, A., HABERMANN, B. H. & SCHNORRER, F. 2015.
1137 The RNA-binding protein Arrest (Bruno) regulates alternative splicing to enable myofibril
1138 maturation in Drosophila flight muscle. *EMBO Rep,* 16**,** 178-91.
1139 SPLETTER, M. L., BARZ, C., YEROSLAVIZ, A., ZHANG, X., LEMKE, S. B., BONNARD, A.,
1140 BRUNNER, E., CARDONE, G., BASLER, K., HABERMANN, B. H. & SCHNORRER, F.
1141 2018. A transcriptomics resource reveals a transcriptional transition during ordered
1142 sarcomere morphogenesis in flight muscle. *Elife,* 7.
1143 STEELE-STALLARD, H. B., PINTON, L., SARCAR, S., OZDEMIR, T., MAFFIOLETTI, S. M.,
1144 ZAMMIT, P. S. & TEDESCO, F. S. 2018. Modeling Skeletal Muscle Laminopathies Using
1145 Human Induced Pluripotent Stem Cells Carrying Pathogenic LMNA Mutations. *Front*
1146 *Physiol,* 9**,** 1332.
1147 SUSSMAN, M. A., BAQUE, S., UHM, C. S., DANIELS, M. P., PRICE, R. L., SIMPSON, D.,
1148 TERRACIO, L. & KEDES, L. 1998. Altered expression of tropomodulin in cardiomyocytes
1149 disrupts the sarcomeric structure of myofibrils. *Circ Res,* 82**,** 94-105.

1150 SWEENEY, H. L. & HAMMERS, D. W. 2018. Muscle Contraction. *Cold Spring Harb Perspect*
1151 *Biol,* 10.
1152 SZIKORA, S., GOROG, P. & MIHALY, J. 2022. The Mechanisms of Thin Filament Assembly
1153 and Length Regulation in Muscles. *Int J Mol Sci,* 23.
1154 TALBOT, J. & MAVES, L. 2016. Skeletal muscle fiber type: using insights from muscle
1155 developmental biology to dissect targets for susceptibility and resistance to muscle
1156 disease. *Wiley Interdiscip Rev Dev Biol,* 5**,** 518-34.
1157 VERHEYEN, E. M. & COOLEY, L. 1994. Profilin mutations disrupt multiple actin-dependent
1158 processes during Drosophila development. *Development,* 120**,** 717-28.
1159 VISA, N. & PERCIPALLE, P. 2010. Nuclear functions of actin. *Cold Spring Harb Perspect Biol,*
1160 2**,** a000620.
1161 WANG, W., LUO, J. & CARROLL, T. 2022. Rfastp: An Ultra-Fast and All-in-One Fastq
1162 Preprocessor (Quality Control, Adapter, low quality and polyX trimming) and UMI
1163 Sequence Parsing). R package version 1.6.0. ed.
1164 WEBER, A., PENNISE, C. R., BABCOCK, G. G. & FOWLER, V. M. 1994. Tropomodulin caps
1165 the pointed ends of actin filaments. *J Cell Biol,* 127**,** 1627-35.
1166 WEITKUNAT, M., KAYA-COPUR, A., GRILL, S. W. & SCHNORRER, F. 2014. Tension and
1167 force-resistant attachment are essential for myofibrillogenesis in Drosophila flight muscle.
1168 *Curr Biol,* 24**,** 705-16.
1169 WICKHAM, H. 2016. ggplot2: Elegant Graphics for Data Analysis.: Springer-Verlag New York.
1170 WILLIAMS, P. E. & GOLDSPINK, G. 1971. Longitudinal growth of striated muscle fibres. *J Cell*
1171 *Sci,* 9**,** 751-67.
1172 WINDNER, S. E., MANHART, A., BROWN, A., MOGILNER, A. & BAYLIES, M. K. 2019.
1173 Nuclear Scaling Is Coordinated among Individual Nuclei in Multinucleated Muscle Fibers.
1174 *Dev Cell,* 49**,** 48-62 e3.
1175 WINTER, J. M., JOUREAU, B., LEE, E. J., KISS, B., YUEN, M., GUPTA, V. A., PAPPAS, C.
1176 T., GREGORIO, C. C., STIENEN, G. J., EDVARDSON, S., WALLGREN-PETTERSSON,
1177 C., LEHTOKARI, V. L., PELIN, K., MALFATTI, E., ROMERO, N. B., ENGELEN, B. G.,
1178 VOERMANS, N. C., DONKERVOORT, S., BONNEMANN, C. G., CLARKE, N. F.,
1179 BEGGS, A. H., GRANZIER, H. & OTTENHEIJM, C. A. 2016. Mutation-specific effects on
1180 thin filament length in thin filament myopathy. *Ann Neurol,* 79**,** 959-69.
1181 YAMASHIRO, S., GOKHIN, D. S., KIMURA, S., NOWAK, R. B. & FOWLER, V. M. 2012.
1182 Tropomodulins: pointed-end capping proteins that regulate actin filament architecture in
1183 diverse cell types. *Cytoskeleton (Hoboken),* 69**,** 337-70.

1184 YAMASHIRO, S., GOKHIN, D. S., SUI, Z., BERGERON, S. E., RUBENSTEIN, P. A. &
1185 FOWLER, V. M. 2014. Differential actin-regulatory activities of Tropomodulin1 and
1186 Tropomodulin3 with diverse tropomyosin and actin isoforms. *J Biol Chem,* 289**,** 11616-
1187 11629.
1188 YAMASHIRO, S., SPEICHER, K. D., SPEICHER, D. W. & FOWLER, V. M. 2010. Mammalian
1189 tropomodulins nucleate actin polymerization via their actin monomer binding and filament
1190 pointed end-capping activities. *J Biol Chem,* 285**,** 33265-33280.
1191 YOUNG, M. D., WAKEFIELD, M. J., SMYTH, G. K. & OSHLACK, A. 2010. Gene ontology
1192 analysis for RNA-seq: accounting for selection bias. *Genome Biol,* 11**,** R14.
1193 YUEN, M., SANDARADURA, S. A., DOWLING, J. J., KOSTYUKOVA, A. S., MOROZ, N.,
1194 QUINLAN, K. G., LEHTOKARI, V. L., RAVENSCROFT, G., TODD, E. J., CEYHAN-
1195 BIRSOY, O., GOKHIN, D. S., MALUENDA, J., LEK, M., NOLENT, F., PAPPAS, C. T.,
1196 NOVAK, S. M., D'AMICO, A., MALFATTI, E., THOMAS, B. P., GABRIEL, S. B., GUPTA,
1197 N., DALY, M. J., ILKOVSKI, B., HOUWELING, P. J., DAVIDSON, A. E., SWANSON, L.
1198 C., BROWNSTEIN, C. A., GUPTA, V. A., MEDNE, L., SHANNON, P., MARTIN, N., BICK,
1199 D. P., FLISBERG, A., HOLMBERG, E., VAN DEN BERGH, P., LAPUNZINA, P.,
1200 WADDELL, L. B., SLOBODA, D. D., BERTINI, E., CHITAYAT, D., TELFER, W. R.,
1201 LAQUERRIERE, A., GREGORIO, C. C., OTTENHEIJM, C. A., BONNEMANN, C. G.,
1202 PELIN, K., BEGGS, A. H., HAYASHI, Y. K., ROMERO, N. B., LAING, N. G., NISHINO, I.,
1203 WALLGREN-PETTERSSON, C., MELKI, J., FOWLER, V. M., MACARTHUR, D. G.,
1204 NORTH, K. N. & CLARKE, N. F. 2014. Leiomodin-3 dysfunction results in thin filament
1205 disorganization and nemaline myopathy. *J Clin Invest,* 124**,** 4693-708.
1206 ZHENG, Y., BUCHWALTER, R. A., ZHENG, C., WIGHT, E. M., CHEN, J. V. & MEGRAW, T.
1207 L. 2020. A perinuclear microtubule-organizing centre controls nuclear positioning and
1208 basement membrane secretion. *Nat Cell Biol,* 22**,** 297-309.
1209